Remote Sensing of Environment 248 (2020) 111960

Contents lists available at ScienceDirect

Remote Sensing of Environment

journal homepage: www.elsevier.com/locate/rse

Remote sensing phenological monitoring framework to characterize corn and soybean physiological growing stages

Chunyuan Diao

Department of Geography and Geographic Information Science, University of Illinois at Urbana-Champaign, Urbana, IL 61801, USA.

ARTICLE INFO

Keywords:
Time series analysis
MODIS
Phenology
Agriculture
Crop progress

ABSTRACT

The phenological dynamics of crops reflect the response and feedback of agricultural systems to climate and environmental constraints, and have significant controls on carbon and nutrient cycling across the globe. Remote monitoring of crop phenological dynamics in a consistent and systematic manner is vitally crucial for optimizing the farm management activities and evaluating the agricultural resilience to extreme weather conditions and future climate change. Yet our ability to retrieve crop growing stages with satellite time series is limited. The remotely sensed phenological transition dates may not be characteristic of crop physiological growing stages. The objective of this study is to develop a remote sensing phenological monitoring framework that can reconcile satellite-based phenological measures with ground-based crop growing observations, with corn and soybean in Illinois as a case study. The framework comprises three key components: time series phenological pre-processing, time series phenological modeling, and time series phenological characterization. As an exploratory prototype, the framework retrieved a total of 56 phenological transition dates that were subsequently evaluated with the district-level ground phenological observations. The results indicated that the devised framework can adequately retrieve a wide range of physiological growing stages for corn and soybean in Illinois, with R square greater than 0.6 and RMSE less than 1 week for most stages. The devised framework largely extends the limited satellite phenological measures to a range of phenological transition dates that are characteristic of essential crop growing stages. It paves the way for formulating standard crop phenological monitoring protocols via remote sensing. The wealth of retrieved phenological characteristics open up unique opportunities to enhance our understanding of the complex mechanisms underlying the crop growth in response to varying environmental stresses, and to make more adaptive farm management strategies towards sustained agricultural development.

1. Introduction

The phenological dynamics of vegetated ecosystems reflect the response and feedback of the terrestrial biosphere to climate and environmental constraints, and have significant controls on matter and energy exchange across the globe (Cleland et al., 2007; Jeong et al., 2011; Morisette et al., 2009; Thackeray et al., 2016). Accurate measurements of intra- and inter-annual changes in vegetation activities exert a marked role in understanding carbon, water, and energy fluxes, evaluating vegetative responses to climate change and variability, and predicting ecosystem changes at local, regional, and global scales (Asner et al., 2000; Diao, 2019a; Diao and Wang, 2016; Kramer et al., 2000; Xie et al., 2018). As a sensitive and integrated indicator of crop growth to environmental conditions, crop phenology has important implications for farm management practices and crop yield predictions (Diao, 2019b; Gao et al., 2017; Sakamoto et al., 2013).

The biophysical structures of crops and their physiological responses (e.g., light use efficiency, photosynthesis, and evapotranspiration) to extreme weather conditions vary across crop growing stages (Brown et al., 2012; Sakamoto et al., 2011). For example, the silking growing stage of corn and the setting pods growing stage of soybean are particularly sensitive to water stress for yield loss, and are regarded as the critical timing for scheduling the irrigation activities (Hickman and Shroyer, 1994; Kilgore and Fjell, 1997). Each day of drought stress may decrease the yield of corn by 3-8% during its silking stage, and reduce the number of pods up to 20% during the setting pods stage of soybean (Lauer, 2012). As a critical link between environmental conditions and yield estimations, crop phenology is an vital constituent in crop models to estimate crop growth conditions, understand seasonal carbon and nutrient cycling, and evaluate crop net primary production (Bolton and Friedl, 2013; Jin et al., 2017; Lokupitiya et al., 2009; Zhang and Zhang, 2016). Hence, remote detection of crop phenological dynamics in a consistent and systematic manner is vitally crucial for optimizing the farm management activities and evaluating

E-mail address: chunyuan@illinois.edu.

https://doi.org/10.1016/j.rse.2020.111960
Received 17 September 2019; Received in revised form 17 June 2020; Accepted 18 June 2020

the agricultural resilience to extreme weather conditions and climate change.

Documenting the phenological progress of crops throughout the growing season over wide geographical regions is an important but challenging task. To date, the most comprehensive ground-based crop phenological progress information at district to state levels is provided by National Agricultural Statistics Service (NASS), United States Department of Agriculture (USDA). Approximately 4000 ground observers throughout the US record the field growing stages of various crops according to NASS phenological observation protocols. Those field observations are compiled to multi-county agricultural statistics district (ASD) or state levels to be published in Crop Progress Reports (CPRs). The CPRs summarize the percentage of specific crops going into certain phenological growing stages (e.g., silking stage of corn) on a weekly basis throughout the growing season. Despite the popularity of CPRs in guiding farm practices and management activities, the ground-based phenological surveys are expensive, time-consuming, and subject to observers' personal assessment. The intensive field reconnaissance makes the ground-based phenological measures impractical for crop phenological monitoring over large geographical regions through time. Besides, the phenological aggregates for a number of counties (or the entire state) roughly summarized in CPRs are insufficient to uncover detailed spatio-temporal phenological patterns at local scales, which makes it challenging to assess crop phenological development under various farming practices (e.g., new cultivars and irrigation strategies) and environmental conditions. Thus a more comprehensive crop phenological monitoring framework that can accommodate the spatio-temporal phenological variations is to be developed.

The recent advances in remotely sensed time series analysis provide unique opportunities to monitor crop phenological progress over space and time. With the satellite time series, a multitude of image compositing and filtering algorithms (e.g., Maximum Value Composite, Best Index Slope Extraction, and Mean Value Iteration) have been devised to reduce the influence of viewing geometry, atmospheric interference and cloud contamination (Julitta et al., 2014; Ma and Veroustraete, 2006; Viovy et al., 1992). Those filtering algorithms reduce the outlying effects mostly through conducting statistical evaluations (e.g., residuals outside a certain statistical range), or assessing the influence of relevant remotely sensed physical processes (e.g., the influence of path radiance). To track the temporal phenological trajectory of crops throughout the growing season, several curve-fitting based phenological models have been devised in recent years, such as Fourier analysis, double logistic function, asymmetric Gaussian function, and smoothing spline function (Hermance et al., 2007; Jönsson and Eklundh, 2004; Zhang et al., 2003; Zhou et al., 2015). Those curve-fitting based models typically fit smoothing curves with given mathematical formulas to the time series of vegetation index (e.g., normalized difference vegetation index [NDVI]). They can further smooth out noise and fluctuations in the satellite time series, as well as uncover the temporal phenological patterns of crops over the course of a year.

With the smoothed satellite time series, the critical phenological transition dates of crop growing stages can be retrieved using phenophase retrieval algorithms (e.g., inflection point algorithms and threshold-defined algorithms) (Boschetti et al., 2009; Moulin et al., 1997; Reed et al., 1994; Wardlow et al., 2006; White et al., 1997). Those algorithms mostly capture the characteristic phenology of crops (e.g., onset or end of growing season) by defining certain thresholds of vegetation index, or detecting the inflection (or transition) points of satellite time series (e.g., derivative of the curve). However, those remotely sensed phenological characteristics have not been adequately adopted in agronomy or crop science studies due to three challenges. First, the remotely detected phenological characteristics (e.g., onset of growing season) are not obviously linked to crop physiological development stages (e.g., emergence or silking growing stages of corn). It is noted that there are timing gaps between the satellite retrieved green-up dates and the ground-measured emergence stage of corn (or soybean), and between the satellite detected dormancy dates and the ground-based harvest stage of corn (or soybean) (Gao et al., 2017). Sakamoto et al. (2010) developed a two-step filtering approach to link the satellite- and ground-based phenological measures, through defining a shape model with critical phenological transition dates. Yet the definition and calibration of the shape model require ancillary ground-based crop phenological growth data, which may not be available over extended geographical regions. Second, most of remotely sensed crop phenological studies are constrained to limited crop physiological growing stages, particularly the emergence and harvest stages of crops, as those stages are more connected to the onset and end of growing season estimated by remote sensing. With the continuing advances in remote sensing, a more systematic framework that can extend the limited satellite phenological measures to a broader range of crop growing stages is to be explored. Third, the remotely sensed phenological characteristics have not been appropriately validated with field-based crop phenological observations. The disparity between spatial coverage of satellite pixels and site-specific field observations, along with the intensive fieldwork in collecting year-long crop phenological observations, makes the remotely sensed phenological validation difficult. Though remotely sensed time series has been demonstrated to be capable of characterizing the seasonal pattern of crop phenological development, few studies have quantitatively evaluated the accuracy of the retrieved phenological characteristics.

The objective of this study is to prototype a remote sensing phenological monitoring framework that reconciles satellite time series phenological measures with ground-based observations to monitor the crop phenological development. With corn and soybean in Illinois as a case study, we specifically seek to: 1) devise a remotely sensed crop phenological monitoring framework to retrieve a wide range of crop growing stages using satellite time series, 2) evaluate a combination of curve-fitting based phenological models and phenophase estimation methods in capturing the crop phenological characteristics, and 3) investigate the relationships between a wide range of remotely sensed phenological characteristics and CPR-based ground crop development stages.

2. Study area and data

2.1. Study area

The study area is Illinois in the Midwest region of United States. Illinois is located in the interior plains with flat terrain and a mean elevation of 180m above sea level. It has a humid continental climate with large temperature differences across seasons. The average temperature in summer is about 23 °C, and the average temperature in winter is around 0 °C. The precipitation is relatively well distributed over the seasons, with its annual average ranging from around 1200mm in the southern portion of Illinois to about 890mm in the north. As a primary agricultural state, Illinois is listed among the top in agricultural productivity and is a major source of agricultural commodities exported from the US. Two major agricultural crops in Illinois are corn and soybean, which are usually rotated in successive years and cultivated in rainfed conditions. The sowing time of corn or soybean varies across years and locations, which largely relies on temperature conditions, soil moisture, and farm management decisions. As a result, the phenological timing of corn or soybean reaching a specific growing stage also varies over space and time throughout Illinois. Based on farming practices and climate conditions, Illinois is partitioned into nine ASDs (Fig. 1). Each ASD is composed of multiple geographically contiguous counties that share similar agricultural characteristics.

2.2. Remote sensing data

Aboard the Terra and Aqua satellites, Moderate Resolution Imaging Spectroradiometer (MODIS) can view the entire surface of Earth every 1

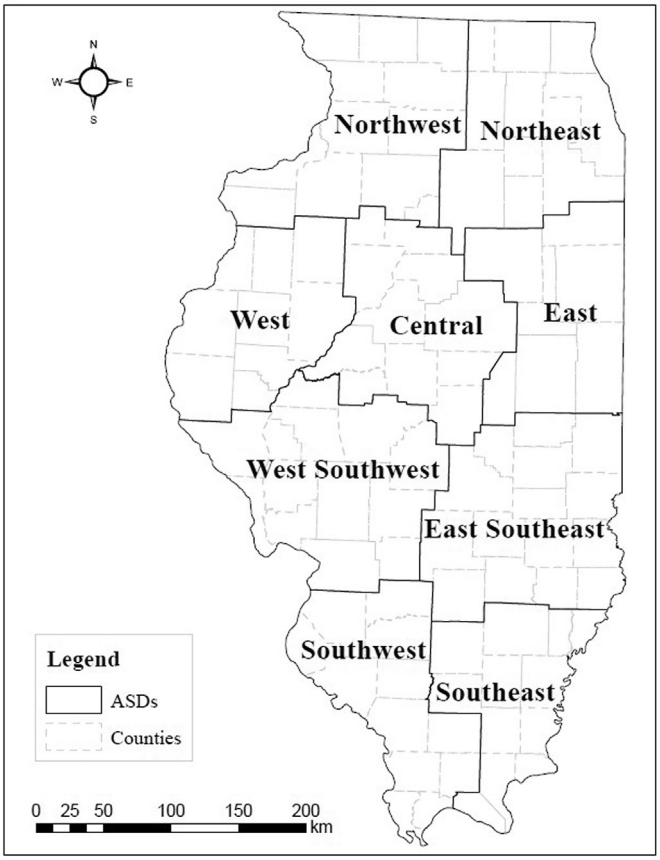

Fig. 1. The agricultural statistics districts of Illinois, US.

to 2 days at spatial resolutions of 250 or 500m. The combination of spatial and temporal resolutions of MODIS represents an appropriate tradeoff to track seasonal dynamic changes of agricultural crops over wide geographical regions. The MODIS MCD43A4 (version 6) nadir Bidirectional Reflectance Distribution Function (BRDF) adjusted reflectance data are collected in this study to build the satellite time series (Schaaf and Wang, 2015b; Schaaf et al., 2002). The MCD43A4 accommodates the viewing angle effects through the BRDF algorithm to retrieve the nadir surface reflectance for MODIS bands 1-7 (i.e., blue, green, red, two near-infrared, and two shortwave-infrared bands). It is a daily 16-day composite dataset and has a 500m spatial resolution. The composite dataset selects the optimal reflectance value for each observation date during its 16-day retrieval period from both Terra and Aqua. The MCD43A4 data are spatially and temporally consistent and comparable, and robust to atmospheric and sensor noise. In this study, the MCD43A4 data covering Illinois over the period 2002-2017 were downloaded from Land Processes Distributed Active Archive Center. As the most widely used vegetation index, NDVI was calculated from the red and near-infrared bands of the MCD43A4 data to build the corresponding satellite time series for phenological analysis.

The MCD43A4 data were pre-processed with ancillary MODIS data (e.g., snow and temperature) to further filter out snow-contaminated and outlying satellite observations. The snow quality assurance layer of the MODIS MCD43A2 (version 6) data was employed to remove the snow-contaminated observations in the data (Schaaf and Wang, 2015a). Additionally, the daily daytime temperature layer of the MODIS MOD11A1 (version 6) land surface temperature data was utilized to flag the winter season in which snow or ice may appear (Wan et al., 2015; Wan et al., 2002). The MCD43A4 data with the daytime surface skin temperature less than 5 °C were labelled as invalid observations (Zhang and Goldberg, 2011). Those flagged spurious or invalid observations of the MCD43A4 data were then substituted by the arithmetic average of valid reflectance values of the close neighbors in the time series. In Illinois, the harvest timings for corn and soybean are usually before winter. The pre-processing of the MCD43A4 is to generate more stable and consistent off-season phenological observations for subsequent analysis.

As two major agricultural crops, corn and soybean are planted in most of the farming area, occupying more than 50% of the land in Illinois. The Cropland Data Layers (CDLs) were used in this study to select relatively pure corn or soybean pixels of the MCD43A4 from 2002 to 2017. The CDLs are produced annually by USDA to map the spatial extents of main crop types in the US at a spatial resolution of 30m (or 56m), and have been used as the cropland reference data in many agricultural studies (Boryan et al., 2011; Johnson and Mueller, 2010). For most of the mapping years in Illinois, the producer's and user's accuracies of corn and soybean classes in CDLs are higher than 90% (NASS CDL, 2018). The CDLs were geographically resized to the MODIS spatial resolution, and the resized pixels with the percentages of corn (or soybean) higher than 90% were retained to build the satellite time series. It is noted that some selected pixels may have lower percentages of corn (or soybean), due to the varying pixel footprint sizes at different view angles of MODIS. As the MCD43A4 product optimizes the daily nadir BRDF-adjusted surface reflectance during its 16-day periods by taking into account observation coverage, image quality, and temporal distance, the pixel purity for the majority of the selected pixels should still be relatively high. The yearly average numbers of relatively pure pixels for corn and soybean per ASD are about 3960 and 1835, respectively.

2.3. Ground-based crop progress reports

To date, the most comprehensive ground-based crop phenological progress and condition data are CPRs, provided by USDA (NASS CPR, 2018). The CPRs present the proportion of main crops reaching certain phenological growing stages at ASD- or state- levels. The description of the surveyed phenological stages for corn and soybean in CPRs is shown in Table 1. For most of the states, the CPRs are only available at the state scale, and those state-level CPRs have served as the main reference data for validating the remotely sensed phenological estimates in previous studies. Yet the spatio-temporal phenological variations across agricultural districts can hardly be accommodated or evaluated. The sampling size of state-level CPRs may not be sufficient to adequately assess the estimation accuracy. In Illinois, the CPRs for corn and soybean are released at both ASD- and state- levels from 2002 to 2017 through the surveys collected from about 127 reporters. For each agricultural district, the area percentage of corn (or soybean) achieving certain growing stages in Table 1 is reported at a weekly interval. For both corn and soybean, this weekly time series of phenological observations was cleaned to ensure the cumulative percentage being monotonically increasing. It was further linearly interpolated to the daily basis to serve as the reference data for validating the remotely sensed phenological estimates. As a tradeoff between the state-level and the site-specific field phenological observations, the ASD-level phenological reference data provide an adequate summary of crop phenological progress over wide geographical regions, as well as accommodate the large-scale spatio-temporal phenological variations within the state.

3. Methods

In this study, we aim to prototype a remote sensing phenological monitoring framework that can reconcile satellite time series phenological measures with ground-based observations to monitor the crop phenological development. The phenological monitoring framework is mainly composed of three components: time series phenological preprocessing (Section 3.1), time series phenological modeling (Section 3.2), and time series phenological characterization (Section 3.3) (Fig. 2). This phenological framework includes a systematic set of

Table 1
Description of phenological development stages for corn and soybean by NASS, USDA.[a]

Corn		Soybean	
Phenological stage	Description	Phenological stage	Description
Emerged	As soon as the plants are visible	Emerged	As soon as the plants are visible
Silking	The emergence of silk like strands from the end of ears	Blooming	A plant should be considered as blooming as soon as one bloom appears.
Dough	Normally half of the kernels are showing dent with some thick or dough-like substance in all kernels.	Setting pods	Pods are developing on the lower nodes with some blooming still occurring on the upper nodes.
Dent	Occurs when all kernels are fully dented and the ear is firm and solid. There is no milk present in most kernels.	Turning yellow	Leaves of soybean start to turn yellow
Mature	Plant is considered safe from frost. Corn is about ready to harvest with shucks opening and there is no green foliage present.	Dropping leaves	Leaves near the bottom of the plant are yellow and dropping, while leaves at the very top may still be green. Leaves are 30-50 percent yellow.
Harvest	Plant is cut, threshed, or otherwise gathered from the field.	Harvest	Plant is cut, threshed, or otherwise gathered from the field.

[a] Adapted from crop progress terms and definitions of NASS, USDA (https://www.nass.usda.gov/Publications/National_Crop_Progress/terms_definitions.php).

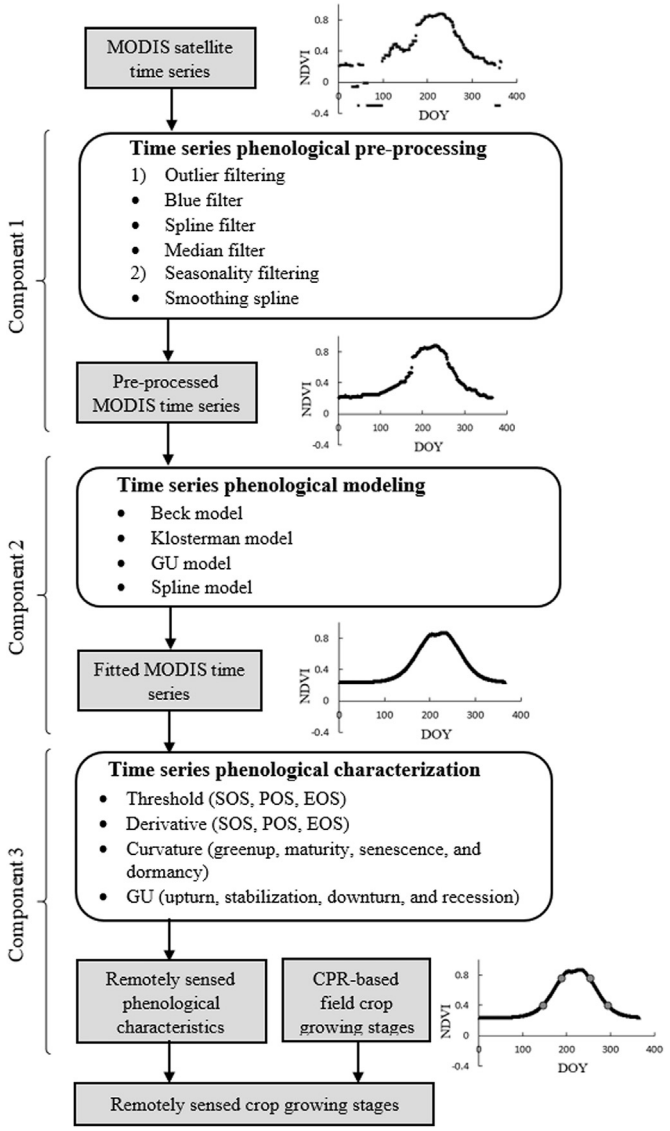

Fig. 2. The remote sensing phenological monitoring framework to characterize crop growing stages.

methodologies that are designed particularly for agricultural phenological monitoring, including seasonality filtering to diminish the influence of weeds and cover crops, double logistic-based phenological models to capture rapid changes in crop growth and development, and diverse phenological characterization methods to retrieve a wide range of crop growing stages. As an exploratory prototype, the framework is designed to encompass the most critical components in crop phenological monitoring, rather than evaluating all the methods in remotely sensed crop phenological studies.

3.1. Time series phenological pre-processing

Due to varying illumination conditions, atmospheric interference, and instrumental noise, the satellite NDVI time series may contain implausible or spurious observations that confound the underlying phenological patterns of crops. As the first component in the phenological monitoring framework, time series phenological pre-processing is to minimize the perturbations of atmospheric and sensor noises, and to smooth the satellite NDVI time series. Specifically, three filtering algorithms, namely blue, spline, and median filters, are devised sequentially in this study to remove the noises in the MCD43A4 NDVI time series of crops.

The blue filtering algorithm is employed to remove the satellite observations that may be contaminated by adverse weather conditions (e.g., snow or cloud) in the MCD43A4 NDVI time series, using the blue chromatic coordinate (BCC) index. The daily BCC index is computed as the reflectance of the blue band divided by the sum of the reflectance of the blue, green, and red bands. The BCC index has been found to be sensitive to changing cloud and snow cover conditions, as the values in the blue band show larger variability during those unstable weather conditions (Julitta et al., 2014). With the daily values, the weekly average and standard deviation of the BCC values can be calculated. Upon testing a multitude of quantiles with reference to previous studies, the study finds that the 5% quantile of the seasonal standard deviation can effectively remove spurious observations while preserving valid ones (Julitta et al., 2014). This quantile is employed to generate a seasonal range of the weekly average BCC values. The satellite observations outside this seasonal range are marked as spurious observations and eliminated from the time series.

After reducing the influence of adverse weather conditions, the spline filtering algorithm is designed to detect and remove outlying satellite observations through statistical evaluations (Migliavacca et al., 2011). The spline filtering algorithm fits a smoothing spline curve to the time series of NDVI and calculates the residuals between the fitted and observed values. A seasonal residual envelope is generated to remove the spurious observations with absolute residual values greater than $\mu + 3\sigma$, where μ and σ are the mean and standard deviation of the residuals, respectively (Migliavacca et al., 2011). The spline filtering algorithm conducts this spline smoothing and residual-based outlier removal recursively until no further outliers are detected.

Finally, the median filtering algorithm is utilized to further smooth the NDVI time series by removing the observations that deviate

considerably from the local trend in the time series (Ganguly et al., 2010). It replaces the NDVI value on each observation date with the median value during its three-day temporal moving window iteratively until there is no change in the time series. With three sequential filtering algorithms, the spurious NDVI observations of the MCD43A4 time series can be further eliminated. Those observations are replaced by the moving average of closest good quality neighbors.

Besides atmospheric and sensor noises, the remotely sensed phenological patterns of target crops (i.e., corn or soybean) may also be confounded by those of off-season vegetation covers (e.g., weeds and cover crops). The off-season in the study denotes the periods before target crops being planted and after target crops being harvested over the course of a year. Though CDLs are used to select relatively pure corn or soybean pixels with a unimodal growing season throughout the year, the weed cover growing before crop planting has been found to affect the remote identification of the green-up onset of crops (Wardlow et al., 2006). To reduce the influence of off-season vegetation covers on the satellite time series, time series phenological pre-processing encompasses a further step for seasonality filtering of the target crops. In this study, the smoothing spline algorithm is employed to smooth out the phenological signals during the off-season by fitting a spline smoothing curve to the satellite observations. The turning points (e.g., peaks and pits) of the smoothed curve segment the satellite time series into different temporal regions. Compared to off-season vegetation covers, the target crops usually achieve higher amplitudes of NDVI with more distinct seasonal dynamics. Thus the range of the growing season of the target crops is estimated as the temporal period delimited by the two constrained surrounding pits of the maximum peak NDVI value of the smoothed curve. The delimiting pits are constrained to the ones with values comparable to off-season NDVI values of the target crops. The local peaks caused by weeds and cover crops were removed and interpolated accordingly through spline functions. As a result, the NDVI values within the estimated range of the growing season are retained or interpolated to minimize the influence of weeds, and the ones outside this range are replaced by the average of the off-season values of the target crops. Under the devised framework, time series phenological pre-processing attempts to improve the spatial and temporal consistency of the MCD43A4 observations for subsequent phenological modeling.

3.2. Time series phenological modeling

After time series phenological pre-processing, time series phenological modeling is designed to model the seasonal phenological development trajectory of crops and uncover their temporal phenological patterns throughout the year. Of the curve-fitting based phenological models, double logistic function has been widely utilized in phenological monitoring, owing to the phenological implications of its estimated parameters and its superior performance to other smoothing algorithms (Zhang et al., 2003). Double logistic function has also been found to model the relatively short growing season better than other algorithms (e.g., asymmetric Gaussian function and Fourier analysis), without overestimating the duration of the growing season (Beck et al., 2006). As agricultural crops usually maintain short growing seasons with rapid changes in vigor from emergence to harvest stages, three types of double logistic-based phenological models, namely Beck, Klosterman, and GU, are devised under the monitoring framework. Those double logistic-based phenological models vary in the number of parameters to be optimized, and thus the flexibility to fit the satellite observations. Additionally, the smoothing spline function is introduced as an alternative in the framework, as it may be more suitable to fit the noisy satellite time series or model the weak phenological patterns (e.g., low seasonal amplitude of NDVI).

The double logistic function assumes that the phenological development of vegetation throughout the year can be represented using two piecewise logistic functions of time (i.e., one function for the upward direction of NDVI, and the other for the downward direction of NDVI) (Zhang et al., 2003). Built upon double logistic function, Beck models the temporal variations in yearly satellite-derived NDVI with six unique parameters that can be interpreted in light of vegetation phenology (Eq. (1)) (Beck et al., 2006).

$$f(t) = a_{base} + (a_{max} - a_{base}) * \left(\frac{1}{1 + e^{(-m_1*(t-m_2))}} + \frac{1}{1 + e^{(n_1*(t-n_2))}} - 1\right) \quad (1)$$

Here, t is the day of year (DOY) and $f(t)$ is the fitted NDVI value at time t using Beck. a_{base} is the off-season NDVI and a_{max} is the maximum NDVI over the course of a year. m_2 and n_2 are the inflection points for the upward and downward directions of NDVI, respectively. m_1 is the rate of increase of the curve at inflection point m_2, and n_1 is the rate of decrease of the curve at inflection point n_2. The off-season NDVI a_{base} is derived according to time series phenological pre-processing in Section 3.1. The other five parameters are estimated via iterative non-linear least squares. Compared to conventional double logistic function, Beck can diminish the impact of spurious observations (particularly caused by snow and ice) on the model fitting process, by replacing all values lower than the off-season NDVI with the off-season NDVI. Beck also has an optional weighting scheme that assigns lower weights to observations overestimated by the fitted curve to track the upper envelop of the observed data. Given the potential positive NDVI bias in the MODIS surface reflectance data, the weighting scheme is not employed in the Beck model. Beck has been demonstrated to be able to model the short growing season of vegetation and to capture abrupt changes of NDVI at the beginning and end of the growing season. Hence it is designed as a candidate model for understanding agricultural phenological dynamics in this study.

Klosterman (Eq. (2)) and GU (Eq. (3)) model the seasonal dynamics of vegetation vigor via more generalized double logistic functions (Gu et al., 2009; Klosterman et al., 2014). These two models incorporate additional parameters to account for diverse and varying vegetation phenological processes over the course of a year, and are more flexible and robust in fitting the seasonal satellite observations. Compared to conventional double logistic function, these models are more capable of tracking diverse phenological trajectories, as they can accommodate different changing rates near the lower and upper asymptotes of the logistic functions, changes of satellite observations during the off-season, non-linear phenological processes during the summer time, etc. Hence, they may provide more accurate model representations of temporal dynamics of crops along the phenological trajectory.

$$\begin{aligned} f(t) &= (a_1 t + b_1) + (a_2 t^2 + b_2 t + c) \\ &\quad * \left[\frac{1}{(1 + m_3 * e^{(-m_1*(t-m_2))})^{m_4}} - \frac{1}{(1 + n_3 * e^{(-n_1*(t-n_2))})^{n_4}}\right] \end{aligned} \quad (2)$$

$$f(t) = a_0 + \frac{a_1}{\left(1 + e^{\left(-\frac{t-m_2}{m_1}\right)}\right)^{m_4}} - \frac{a_2}{\left(1 + e^{\left(-\frac{t-n_2}{n_1}\right)}\right)^{n_4}} \quad (3)$$

Here, t is DOY and $f(t)$ is the fitted NDVI value at time t using Klosterman (Eq. (2)) or GU (Eq. (3)). A more comprehensive set of parameters are taken into account in these two models to represent the phenological processes. The empirical parameters in Klosterman are a_1, b_1, a_2, b_2, c, m_1, m_2, m_3, m_4, n_1, n_2, n_3 and n_4. The empirical parameters in GU are a_0, a_1, a_2, m_1, m_2, m_4, n_1, n_2 and n_4. Klosterman and GU are both generalized double logistic models, yet they vary in the number of parameters to be estimated and thus the flexibility in fitting the satellite observations. In this study, those parameters are optimized to fit the yearly NDVI time series of crops using the phenopix library in R (Filippa et al., 2016).

The smoothing spline function can also model the crop seasonal phenological trajectory, besides being utilized to remove outliers and

diminish the influence of off-season vegetation covers (Section 3.1). It models the seasonal variation of NDVI through fitting piecewise polynomials to temporal segments of data, and joining the polynomials to a continuous curve at the connecting locations of those segments (i.e., knots) (Dierckx, 1995; Hermance et al., 2007). The continuity conditions at the knots typically require the continuity of both the spline curve and its derivatives. The order of polynomial pieces, the number of knots, and the quality of observations regulate the sensitivity of the smoothing spline in modeling the remotely sensed phenological time series. In smoothing splines, the smoothing parameter is utilized to balance the goodness of fit to the data and the level of smoothness of the curve. A lower smoothing parameter indicates higher fidelity to the data and also the chance of overfitting, while a higher smoothing value implies a larger penalty for the roughness of the curve and may lead to underfitting. Hence an appropriate smoothing parameter that adapts to intra-annual phenological fluctuations is important to capture the crop seasonal patterns, suppress spurious oscillation, and avoid overfitting. In this study, the optimal smoothing parameter is estimated by generalized cross validation to fit the observed data to defined level of precision.

The spline model is a data-driven functional representation of vegetation phenological process without the constraints of shape being imposed by other phenological models (e.g., double logistic function). With its more flexible data-driven phenological shape, the spline model may be a desired alternative to capture the weak or complicated crop phenological patterns in the framework. Given the relatively homogenous agricultural fields monitored in this study, the cubic smoothing spline with third-order piecewise polynomials is selected for characterizing the crop phenology. Other spline models, such as regression splines and high-order splines may also be good candidates for phenological estimations, especially in diversified and intensified agricultural systems (Bradley et al., 2007; Hermance et al., 2007).

3.3. Time series phenological characterization

With the smoothed time series curves generated by phenological models, time series phenological characterization is to estimate the critical phenological transition dates that are characteristic of crop physiological growing stages (e.g., emerged and silking stages for corn). In this study, four representative types of phenological characterization methods, namely threshold-based, derivative-based, curvature-based, and Gu-based methods, are devised to retrieve crop phenological transition dates in the framework. With different phenological characterization strategies, those methods may shed light on both shared and distinct crop growing characteristics.

The threshold-based method extracts the critical phenophases of crop development through arbitrary user-defined thresholds (White et al., 2009). The thresholds for phenological characterization can be defined using absolute values (e.g., NDVI being 0.1), or relative values (e.g., NDVI being 10% of its amplitude) (White et al., 1997). Due to the difference in vegetation biochemical and biophysical structures, the absolute thresholds defined for phenophase extractions in one geographical region might not be suitable over extended regions. The relative thresholds, on the other hand, may be more desired to capture the important phenophases by identifying the DOYs when defined percents of the amplitude of NDVI are reached. A range of relative thresholds have been examined in phenological studies with mixed results reported (Gao et al., 2017; Shen et al., 2014; White et al., 1997; Yu et al., 2010). Despite the simple configuration of the threshold-based method, the trials and efforts in defining arbitrary thresholds make this type of method cumbersome to implement in the monitoring of crop growing progress at large scales. In this study, three phenological transition dates, namely start of season (SOS), peak of season (POS), and end of season (EOS), are estimated as the exploratory prototype in the devised framework. The threshold-based SOS and EOS are defined when 50 percents of the amplitude of NDVI are reached during the upward direction and downward direction of the smoothed curve, respectively. The POS is defined when the maximum NDVI of the smoothed curve is achieved. Other thresholds, despite the potentials in phenological characterization, are not studied in the exploratory framework.

The derivative-based method characterizes the crop development according to local extremes in the first derivative of the smoothed time series curve. The rapid changes of NDVI values reflected in the derivative of the curve, associated with drastic changes in vegetation vigor and photosynthetic activities, may be indicative of vegetation phenological transitioning from one stage to another. Those inflection points represented by the derivative of the curve are hence employed for phenological characterization. Similar to the threshold-based method, three phenological transition dates, namely start of season (SOS), peak of season (POS), and end of season (EOS), are estimated using the derivative-based method in the devised framework. The derivative-based SOS and EOS are defined when the first derivative of the smoothed curve achieves the absolute maximum and minimum, respectively. The POS is defined when its first derivative reaches zero between SOS and EOS.

The curvature-based method retrieves the crop phenophases based on the local extremes in the rate of change in the curvature of the fitted phenological model (Klosterman et al., 2014; Zhang et al., 2003). This type of method attempts to estimate the phenological transition dates by capturing the inflection points when the curvature of the fitted NDVI time series changes the most rapidly. In the framework, four transition dates (i.e. greenup, maturity, senescence, and dormancy) are retrieved with the curvature-based method. The greenup and maturity dates correspond to the times when the rate of change in the curvature reaches two local maxima during the upward direction. Those dates indicate the seasonal growth of vegetation transitions from one approximately linear stage to another. Similarly, the senescence and dormancy dates are defined when the rate of curvature change of NDVI time series achieves two local minima in the downward direction.

The Gu-based method captures the crop phenological progress using a combination of boundary lines (e.g., plateau and baseline) and local extremes in the first derivative of the smoothed curve (Gu et al., 2009). The method models the seasonal dynamic trajectory of vegetation as approximately linear processes using recovery and senescence lines. The recovery line is defined as the line that goes through the maximum point of the first derivative of the curve with a slope of peak recovery rate. The peak recovery rate is the maximum value of the first derivative of the curve, which represents the maximum slope in the upward direction of the curve. Correspondingly, the senescence line is defined as the line that passes through the minimum point of the first derivative with a slope of peak senescence rate, and the peak senescence rate is the minimum of the first derivative of the curve. Four phenological transition dates (i.e., upturn, stabilization, downturn, and recession) can be estimated using the Gu-based method accordingly. The upturn and stabilization dates correspond to the times when the recovery line intersects the baseline and the plateau line, respectively. The baseline and the plateau line are further defined as the horizontal lines corresponding to the minimum (i.e., off-season NDVI) and the maximum (i.e., amplitude) of the curve. Similarly, the recession and downturn dates are estimated when the senescence line intersects the baseline and the plateau line, respectively. Those phenological transition dates represent the critical inflection points to mark the transitioning of phenophases when linear growing and senescent processes are assumed to approximate the overall shape of the seasonal cycle of vegetation dynamics.

Those four types of phenological characterization methods retrieve the phenophases according to different curve properties or empirical thresholds. As a result, the phenological transition dates retrieved by different characterization methods may have marked varying ecological meanings. In the devised framework, the diverse phenological characterization methods allow the flexibility of selecting the ones better suited to the phenological trajectory of crops in different agricultural

systems.

3.4. Accuracy assessment

With the combination of time series phenological modeling and time series phenological characterization, a suite of phenological transition dates can be estimated in the devised framework. For all the mapping years, those phenological transition dates were retrieved for all the extracted corn and soybean pixels. The retrieved transition dates were summarized to the ASD level and the cumulative percentages of those transition dates for both corn and soybean throughout the growing season were derived. To assess the alignment between remotely sensed characteristic phenology and ground-based phenological observations, the cumulative percentages of the retrieved transition dates were compared to the percentages of crops reaching corresponding field physiological growing stages. For example, the cumulative percentage of transition dates of POS retrieved by the threshold method was compared to the percentage of corn going into silking, dough, and dent growing stages, respectively. With regard to soybean, the cumulative percentage of transition dates of threshold-derived POS was compared to its percentage entering blooming, setting pods, and turning yellow growing stages, respectively. A complete list of comparisons was in Table 2, with reference to definitions of phenological characteristics of transition dates. Due to the weekly phenological observation interval and the missing data issues in CPRs, we further evaluated the alignment for each comparison by focusing on comparing the median date of the retrieved transition dates (at 50% level of the cumulative distribution) to that of crop reaching the corresponding growing stage across years using the statistical measures of R square and root mean square error (RMSE). This wide range of comparisons were designed to unveil how remotely sensed phenological measures can be reconciled with field-based observations under the phenological monitoring framework.

4. Results

4.1. Remotely sensed phenological characteristics

Under the phenological monitoring framework, time series phenological pre-processing was employed to smooth out spurious satellite observations over the course of a year. Four time series phenological models and four types of time series phenological characterization methods were devised to extract the relevant phenological transition dates that may be indicative of crop physiological growing stages. In total, there were 16 modeling combinations for phenological extractions (Fig. 3). The rows in the figure represented different phenological modeling methods (i.e., Beck, Klosterman, GU, and Spline), and the columns in the figure denoted different phenological characterization methods (i.e., threshold [TR], derivative [DE], curvature [CU], and Gu [GU]). For instance, the combination of Beck - DE denotes that the smoothed satellite observations were fitted using the Beck phenological model, with the phenological transition dates estimated by the derivative-based method. According to Section 3.3, three phenological transition dates (i.e., SOS, POS, and EOS) were estimated using the derivative-based and threshold-based methods, respectively. Four transition dates (i.e., greenup, maturity, senescence, and dormancy) were retrieved with the curvature-based method, and four transition dates (i.e., upturn, stabilization, downtown, and recession) were detected using the Gu-based method. Hence a wide range of phenological characteristics were retrieved under the phenological monitoring framework to facilitate a comprehensive comparison with ground-based phenological measures.

A total of 56 phenological transition dates were estimated under the framework (Fig. 3). For example, with the Beck phenological model and the derivative-based characterization method, the transition dates of SOS, POS, and EOS were estimated. The density distributions of SOS for corn and soybean in Illinois were plotted in Fig. 4. As for corn, the mean transition dates of SOS varied from DOY 155 to 170, with the standard deviation ranging from 6 to 12 days throughout the mapping years. In respect of soybean, the retrieved mean SOS varied from DOY 168 to 187, and the standard deviation across the years was from 6 to 13 days. With the Beck - DE method, the retrieved mean transition dates of SOS for corn were about 1-3 weeks earlier than those estimated for soybean from 2002 to 2017 in Illinois. The density distributions of Beck - DE retrieved POS and EOS for corn and soybean were also derived (Figs. S1 and S2). Similar to SOS, the mean transition dates of POS achieved by corn were earlier than those of soybean for the mapping years in Illinois, with a mean difference of 10-24 days. In contrast, the mean transition dates of EOS estimated for corn were much closer to those of soybean. The absolute mean difference of EOS across the years between corn and soybean was about 1 week (except 2012).

4.2. Field crop phenological measures

In Illinois, field phenological progress for corn and soybean was surveyed and reported at the ASD level in the CPRs. From 2002 to 2017, the median dates of corn and soybean reaching their respective phenological development stages throughout Illinois were shown in Fig. 5. Those median dates of phenological stages for both crops varied from year to year, with relatively earlier dates in 2010 and 2012, and later days in 2008 and 2009. The variations in the timing of crops entering their phenological stages were partly attributable to crop planting time, weather conditions (e.g., cold and wet weather conditions may delay the timing of crops being planted and entering the subsequent stages), soil moisture conditions, and farming practices. Over the mapping years, the mean and standard deviation of the median phenological dates for both crops were summarized in Table 3. Upon comparisons of phenological progress between corn and soybean in Table 3 and Fig. 5, corn emerged about 1-3 weeks earlier than soybean across years, which corresponded to the density distributions of Beck - DE retrieved SOS for

Table 2
Comparisons of remotely sensed phenological characteristics with field crop growing stages.

Corn					Soybean				
Field stage	Remotely sensed characteristic				Field stage	Remotely sensed characteristic			
	Threshold	Derivative	Curvature	Gu		Threshold	Derivative	Curvature	Gu
Emerged	SOS	SOS	Greenup	Upturn	Emerged	SOS	SOS	Greenup	Upturn
Silking	POS	POS	Maturity	Stabilization	Blooming	SOS/POS	SOS/POS	Maturity	Stabilization
Dough	POS	POS	Senescence	Downturn	Setting pods	POS	POS	Maturity /Senescence	Stabilization /Downturn
Dent	POS/EOS	POS/EOS	Senescence	Downturn	Turning yellow	POS/EOS	POS/EOS	Senescence	Downturn
Mature	EOS	EOS	Senescence /Dormancy	Downturn /Recession	Dropping leaves	EOS	EOS	Senescence /Dormancy	Downturn /Recession
Harvest	EOS	EOS	Dormancy	Recession	Harvest	EOS	EOS	Dormancy	Recession

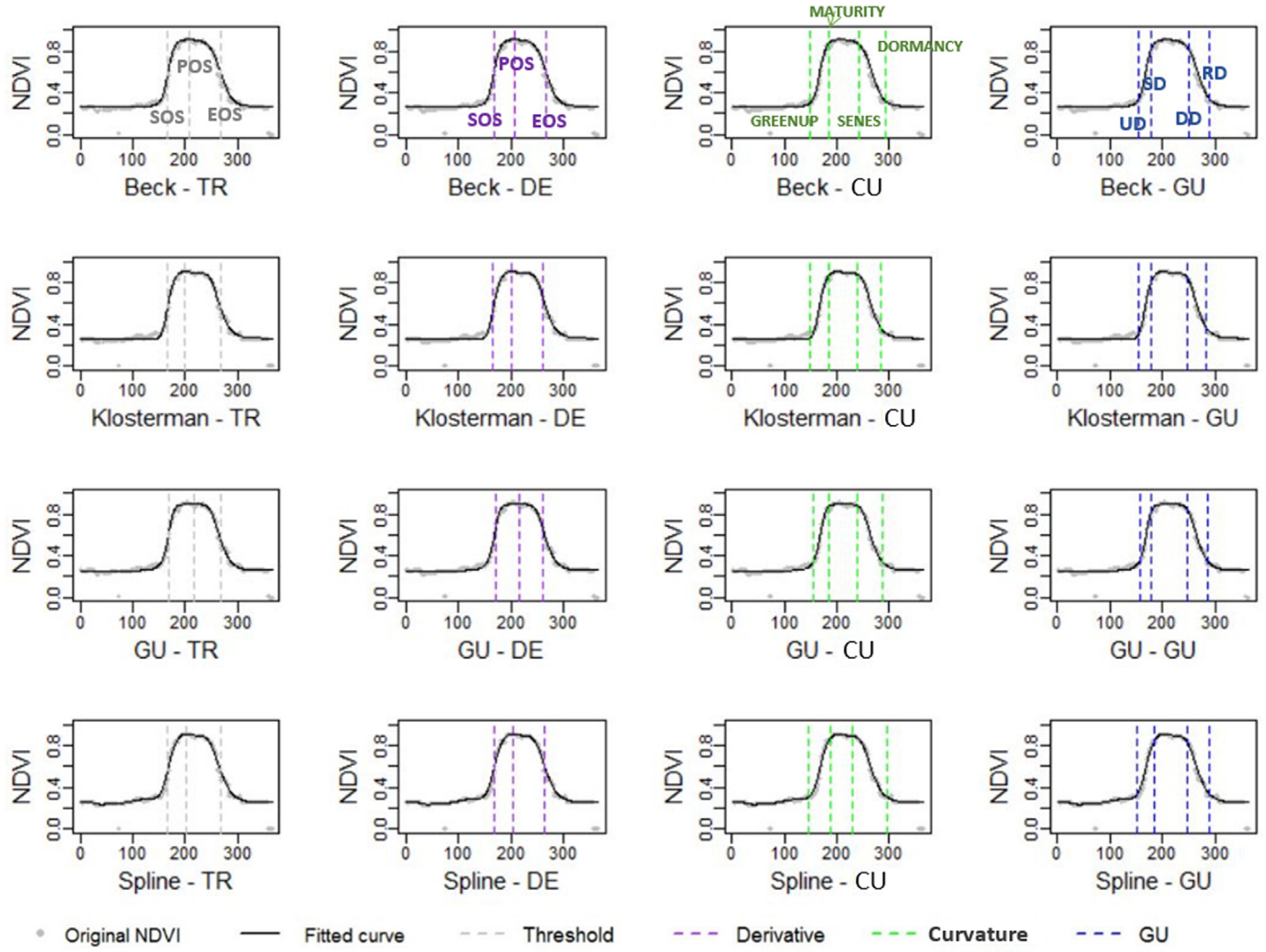

Fig. 3. Phenological characteristics retrieved under the monitoring framework.

those two crops in Fig. 4. Besides, there were multiple comparable timings between those two crops along the phenological development trajectory, including the silking stage of corn and the blooming stage of soybean, the dough stage of corn and the setting pods stage of soybean, the mature stage of corn and the dropping leaves stage of soybean, and the harvest stage of corn and the harvest stage of soybean. Throughout the growing season, the ASD-based ground phenological observations from a wide range of crop development stages in CPRs provide an indispensably essential reference for evaluating the remotely sensed phenological characteristics.

4.3. Characteristic phenology under the monitoring framework

Under the phenological monitoring framework, a wide range of phenological transition dates were retrieved using the four representative phenological characterization methods. The cumulative percentages of the retrieved phenological transition dates over time were calculated for corn and soybean throughout Illinois. Using the Beck-based phenological model as an example, the cumulative percentages of curvature-based greenup dates and Gu-based upturn dates for corn in 2013 aligned with the cumulative percentages of corn going into the emerged stage in CPRs (Fig. 6). The threshold-based and derivative-based SOS dates tended to lie between the emerged and silking stages of corn. The threshold-based POS, derivative-based POS, curvature-based maturity, and Gu-based stabilization dates were around the silking stage of corn in 2013. The cumulative percentages of curvature-based senescence dates and Gu-based downturn dates for corn approached the cumulative percentages of corn reaching the dent stage in ground observations. Also in Fig. 6, the threshold-based and derivative-based EOS dates were linked with the mature stage of corn, and the curvature-based dormancy dates and Gu-based recession dates were connected with the harvest stage of corn. Hence those diverse phenological characteristics unified under the proposed framework could facilitate the remote retrieval of a variety of crop physiological growing stages. Among those four representative types of phenological characterization methods, the cumulative distributions of transition dates from the threshold-based and derivative-based methods (e.g., SOS dates) were comparable in Fig. 6. Additionally, the phenological transition dates from the curvature-based and Gu-based methods (e.g., greenup and upturn dates) were comparable, and exhibited similar alignments with ground-based measures.

To facilitate a more comprehensive comparison between the remotely sensed phenological characteristics and ground-based crop phenological measures, the cumulative percentages of phenological transition dates for all the mapping years (2002 to 2017) were calculated (e.g., Figs. 7 and 8 for corn, and Figs. 9 and 10 for soybean using the Beck phenological model). Due to the large amount of devised phenological characteristics, the transition dates from the same phenological characterization methods were shown in same colors. For example, all the transition dates (i.e. SOS, POS, and EOS) from the

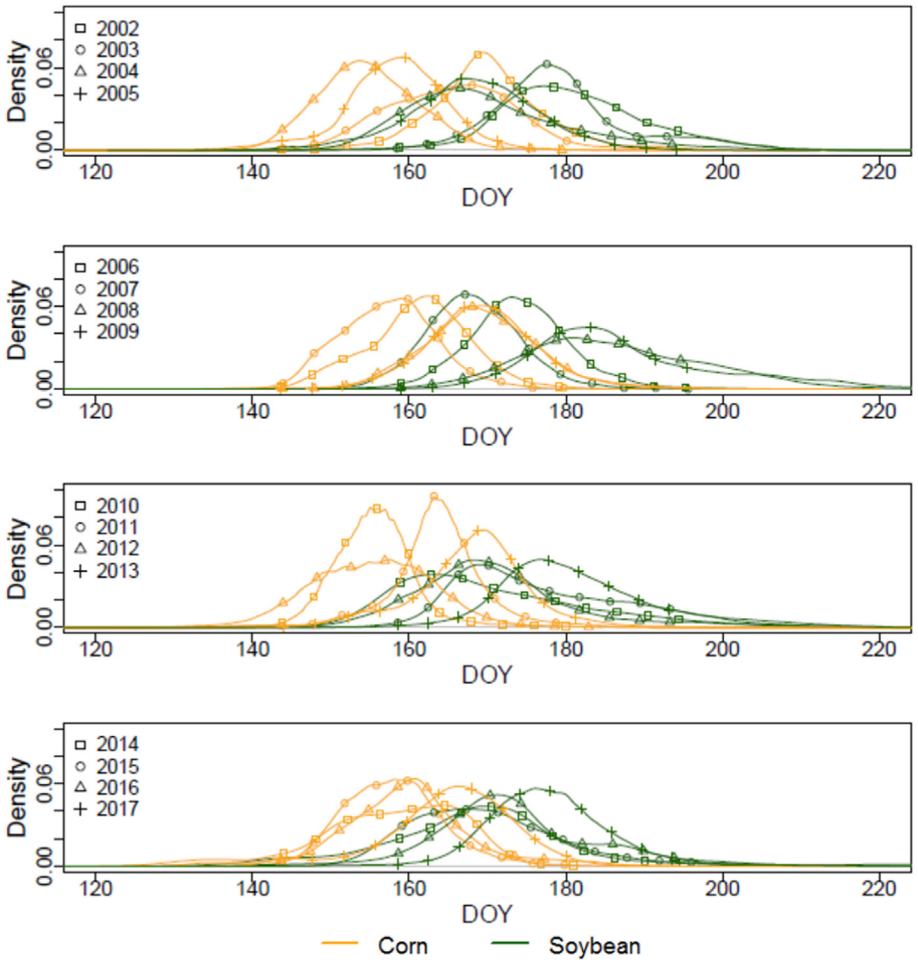

Fig. 4. The transition dates of SOS estimated by the Beck phenological model and the derivative-based characterization method for corn and soybean.

derivative-based method were colored in purple, with the time sequence following that in Fig. 6. With respect to corn, the phenological characteristics captured under the framework showed relatively consistent alignment patterns across years. From 2002 to 2017, the curvature-based greenup dates and Gu-based upturn dates were closely linked to the emerged stage of corn. The curvature-based maturity dates

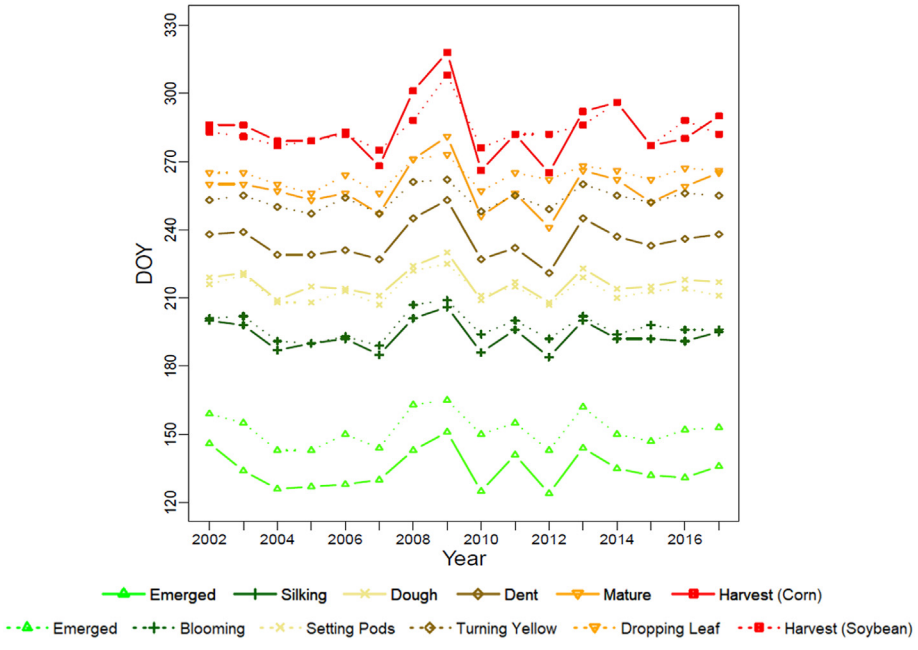

Fig. 5. The field phenological growing stages of corn and soybean in Illinois during 2002-2017.

Table 3
The mean and standard deviation of the median observation dates of crop growing stages in Illinois from 2002 to 2017.

Corn			Soybean		
Phenological stage	Mean	Standard deviation	Phenological stage	Mean	Standard deviation
Emerged	135	8	Emerged	152	7
Silking	193	6	Blooming	197	6
Dough	217	6	Setting pods	214	6
Dent	235	8	Turning yellow	254	5
Mature	258	10	Dropping leaves	264	5
Harvest	284	14	Harvest	284	8

and Gu-based stabilization dates were characteristic of its silking stage. The threshold-based POS and derivative-based POS dates were linked to the dough phenological stage. The distribution patterns of curvature-based senescence dates and Gu-based downturn dates were comparable to those of corn going into the dent stage. The threshold-based EOS and derivative-based EOS dates were connected with the mature stage of corn, and the curvature-based dormancy dates and Gu-based recession dates corresponded to its harvest stage. The further overlapping among those four phenological characterization methods indicated that the transition dates of corn extracted by the threshold-based and derivative-based methods were comparable. The curvature-based and Gu-based transition dates showed similar cumulative distribution patterns.

As regards soybean, the phenological transition dates retrieved by the framework also exhibited comparable patterns throughout the mapping years. Similar to corn, the curvature-based greenup dates and Gu-based upturn dates were characteristic of the emerged stage of soybean from 2002 to 2017. The curvature-based maturity dates and Gu-based stabilization dates were connected to its blooming period. The threshold-based and derivative-based POS dates were linked to the setting pods phenological stage. The curvature-based senescence dates and Gu-based downturn dates had implications for the turning yellow stage of soybean. The cumulative distributions of threshold-based and derivative-based EOS dates were indicative of its dropping leaves stage. The curvature-based dormancy dates and Gu-based recession dates aligned with the timing of soybean reaching its harvest stage. Comparable to the ground-based phenological observations, the cumulative percentages of those transition dates showed logistic patterns, except the curvature-based maturity dates. This deviation may be attributable to the shorter growing seasons of soybean, which complicated the detection of the inflection maturity point from the fitted curve. Resonating with corn, the threshold-based and derivative-based methods retrieved similar phenological characteristics, and the curvature-based and Gu-based methods captured comparable phenological transition dates.

4.4. Reconciling remotely sensed with ground-based phenological measures

Due to the weekly phenological observation interval and the missing data issues in CPRs, we further evaluated the satellite versus ground-based phenological measures by focusing on calculating the difference between the median of the retrieved phenological transition dates and the median dates of crops reaching specific growing stages. For instance, with the Beck phenological model and the Gu-based characterization method, the medians of the four transition dates (i.e., upturn, stabilization, downturn, and recession dates) were compared against the median dates of corn reaching the emerged, silking, dent, and harvest stages, respectively (Fig. 11). As for soybean, the medians of those transition dates were compared to the median dates of soybean going into the emerged, blooming, turning yellow, and harvest stages, respectively. According to Section 4.3, those phenological growing stages were the most relevant stages to the Gu-derived measures. Those comparisons were conducted at the ASD level, with the yearly satellite versus ground-based median pairs as observations in Fig. 11. The one-to-one line in the figure indicated that the remotely sensed and ground-based median pairs aligned with each other exactly. For both corn and soybean, most of the median pairs were distributed along the one-to-one line, particularly for the Gu-based downturn versus CPR-based dent median dates of corn, and the Gu-based stabilization versus CPR-based blooming median dates of soybean. The distribution patterns of the Beck-Gu based median pairs in Fig. 11 exhibited similar trends as the cumulative distribution patterns of the Beck-Gu derived measures in Figs. 7, 8, 9 and 10.

The four phenological models (i.e., Beck, Klosterman, GU, and Spline) were all retained for the comparisons (Figs. 12 and 13), as they had comparable fitting results to NDVI observations after time series phenological pre-processing under the framework. The mean RMSE

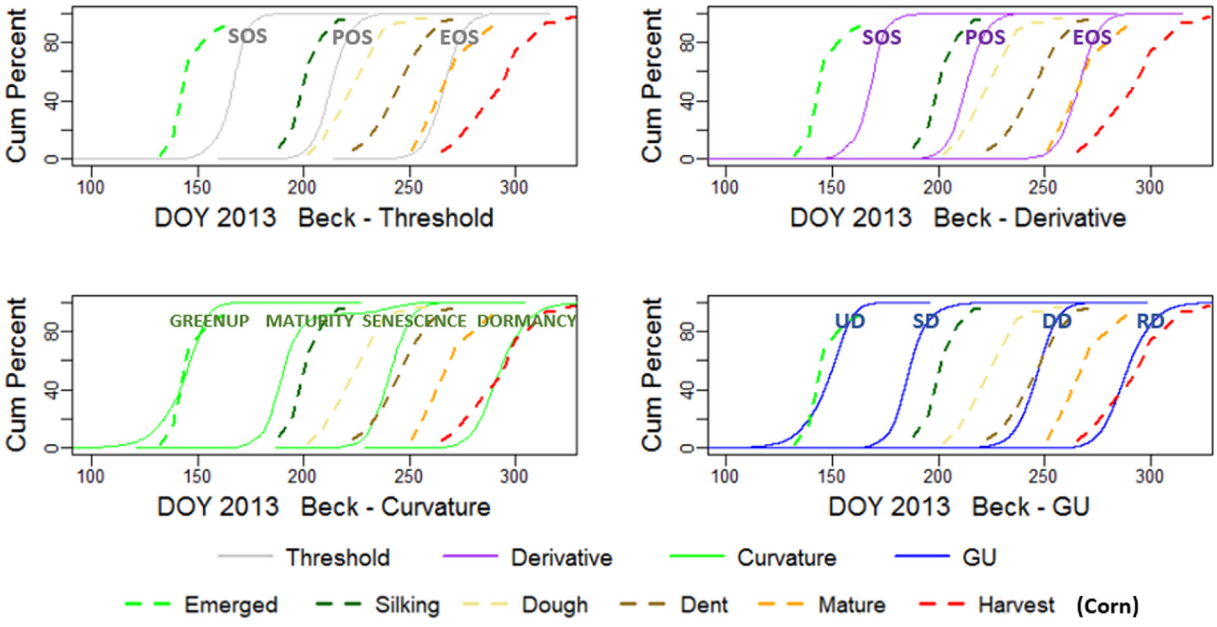

Fig. 6. The cumulative percentages of phenological transition dates of corn retrieved by the Beck phenological model and four types of phenological characterization methods in 2013 throughout Illinois.

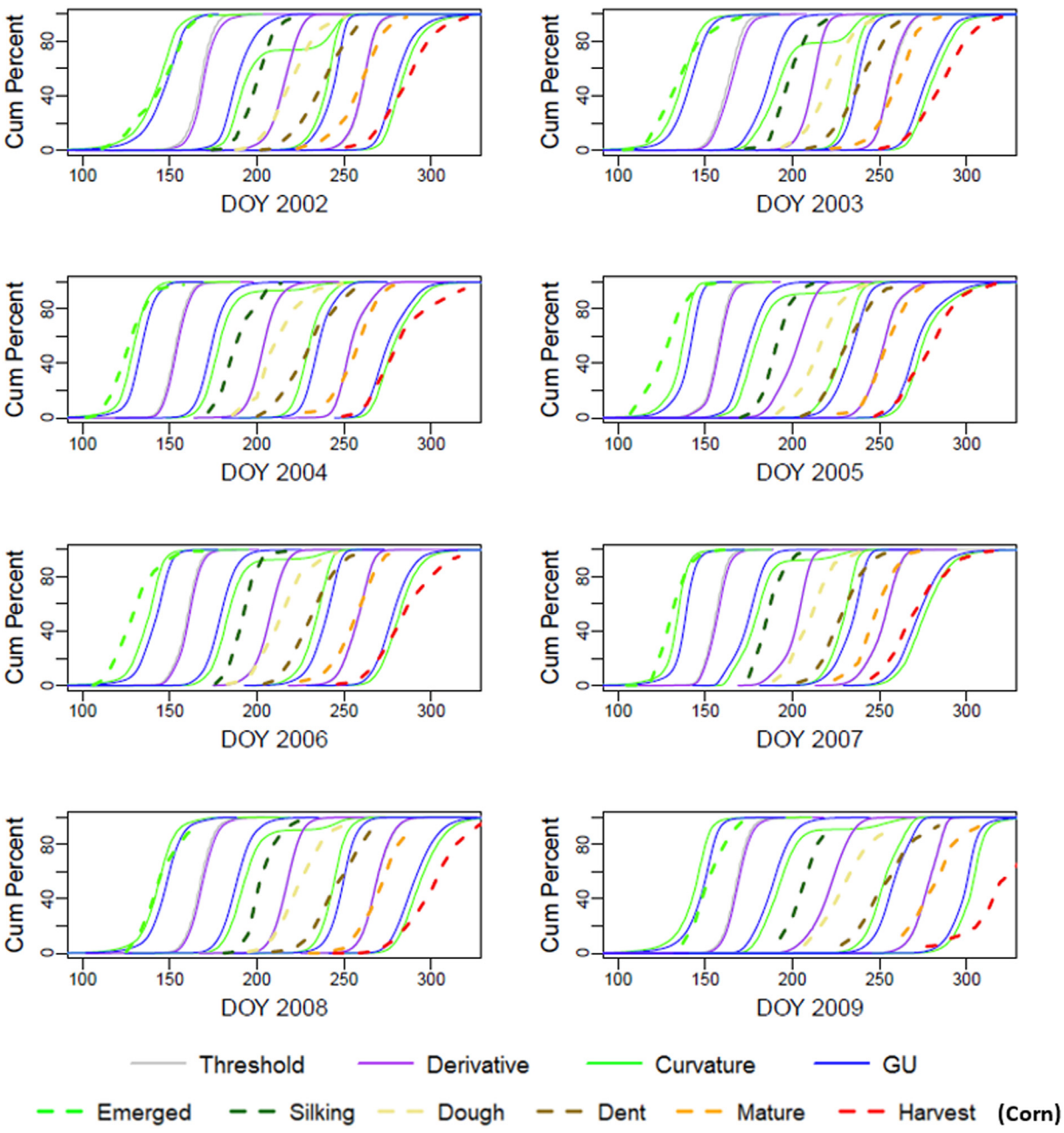

Fig. 7. The cumulative distributions of satellite-Beck-retrieved versus CPR-based crop phenological stages of corn from 2002 to 2009 throughout Illinois.

values between the fitted and observed NDVI throughout Illinois for the Beck, Klosterman, GU, and Spline methods were 0.019, 0.023, 0.021, and 0.019, respectively. Those four phenological models were colored differently in Figs. 12 and 13. According to Table 2, the median date of corn going into the emerged stage was compared to the medians of the threshold-based SOS, derivative-based SOS, curvature-based greenup, and Gu-based upturn dates (Fig. 12). Among those transition dates, the curvature-based greenup and Gu-based upturn dates showed lower RMSE values (about 6.08-14.09 days), along with relatively high R square values (about 0.58-0.68), particularly from the spline phenological model. It indicated that more than 58 percent of variability in the median dates of the field-based emerged stage of corn could be explained by the devised phenological characteristics under the framework. The average of the difference between the remotely retrieved and field-based emergence measures was less than 2 weeks. Correspondingly, the comparisons were made for the other phenological growing stages and the results were in Fig. 12.

Across a wide range of corn development stages, the Beck phenological model maintained relatively good performance in retrieving the transition dates, particularly for the silking, dough, dent, and mature stages of corn. It achieved relatively high R square values and low RMSE values. Different phenological characterization methods might give rise to varying detection accuracies. With the dent stage of corn as an example, the RMSE values ranged from 5.62 to 27.23 days through phenological characterization methods (Fig. 12). This retrieval difference from the curvature-based senescence dates (less than 1 week difference) to the threshold-based POS dates (more than 3 weeks difference) emphasized the importance of selecting the appropriate characterization methods in phenological estimations. Upon comparisons, the most suitable combinations of phenological modeling and characterization methods for estimating the corn physiological growing stages under the framework were shown in Table 4. Most of the combinations had R square values greater than 0.65, and RMSE less than 11 days. Considering the weekly observation interval of CPRs and the

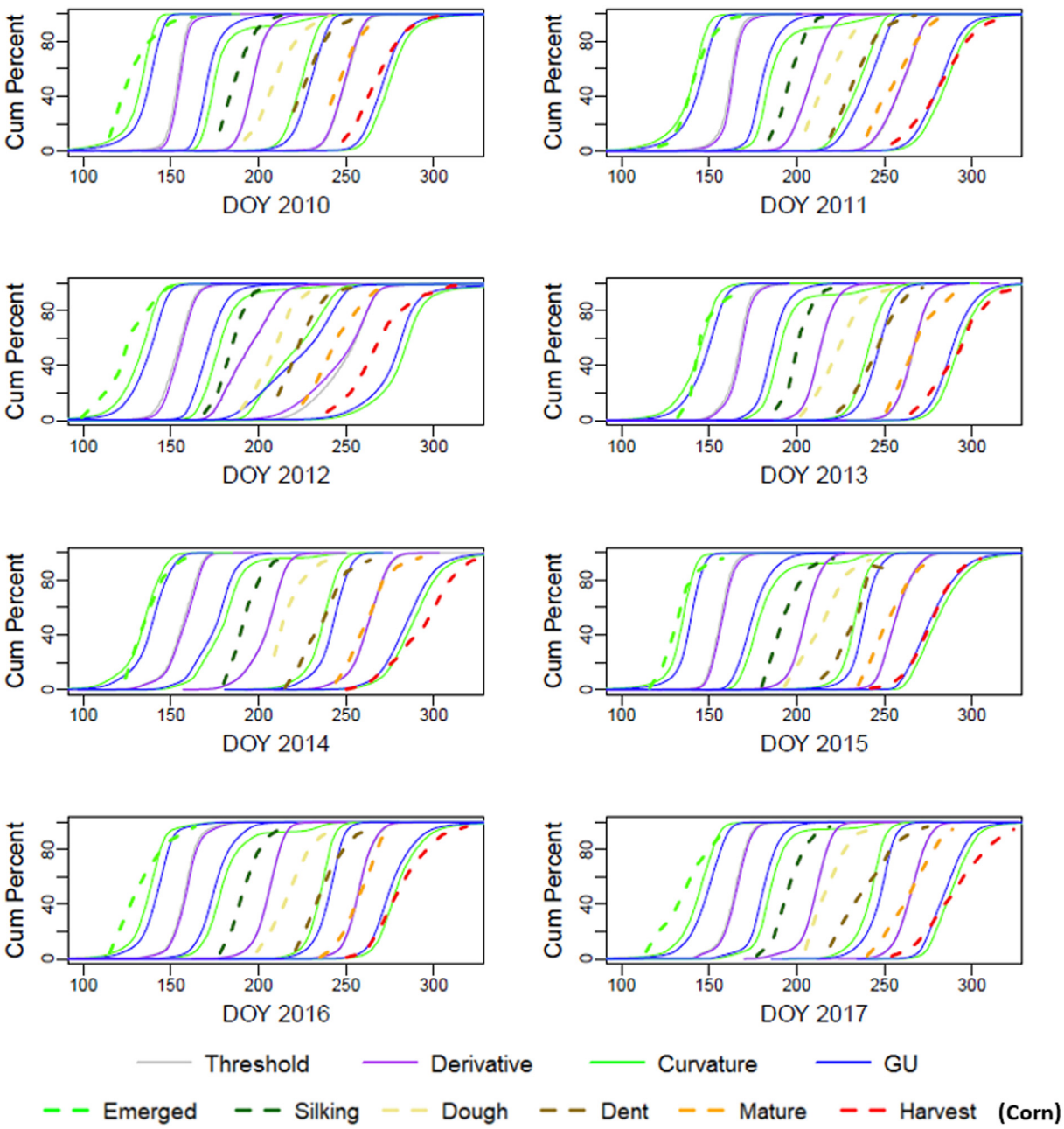

Fig. 8. The cumulative distributions of satellite-Beck-retrieved versus CPR-based crop phenological stages of corn from 2010 to 2017 throughout Illinois.

compositing process in the MODIS data, the 11-day (or less) difference should be adequate for demonstrating the capabilities of the framework in conducting systematic, consistent, and repetitive phenological monitoring.

Additionally, the median dates of soybean reaching the phenological growing stages were compared to the medians of corresponding transition dates in Table 2. The R square and RMSE values were calculated and shown in Fig. 13. This suite of desired combinations of phenological modeling and characterization methods yielded varying phenological estimation results, with R square ranging from 0.53 to 0.68 and RMSE from 4.96 to 10.95 days. As in corn, the Beck phenological model exhibited relatively good performance across diverse phenological stages, though the other phenological models might achieve favorable retrieval accuracies for certain phenological stages. By comparisons, the most desirable combinations of phenological modeling and characterization methods for soybean phenological retrieval were in Table 5. For most development stages, the R square values were higher than 0.6 and the RMSE values were less than 11 days. It indicated that the phenological framework could adequately estimate the soybean development stages besides its good performance for corn.

5. Discussion

Encompassing time series phenological pre-processing, time series phenological modeling, and time series phenological characterization, the framework is devised to embrace the most essential components in crop phenological monitoring. This framework evaluated a combination of 56 phenological transition dates in its exploratory prototype, and showed good performance (R square greater than 0.6 and RMSE less than 1 week for most desired combinations) in phenological retrievals for both corn and soybean at the ASD level. The systematic comparisons among the combinations presented a comprehensive roadmap to reconcile the remotely sensed phenological measures with

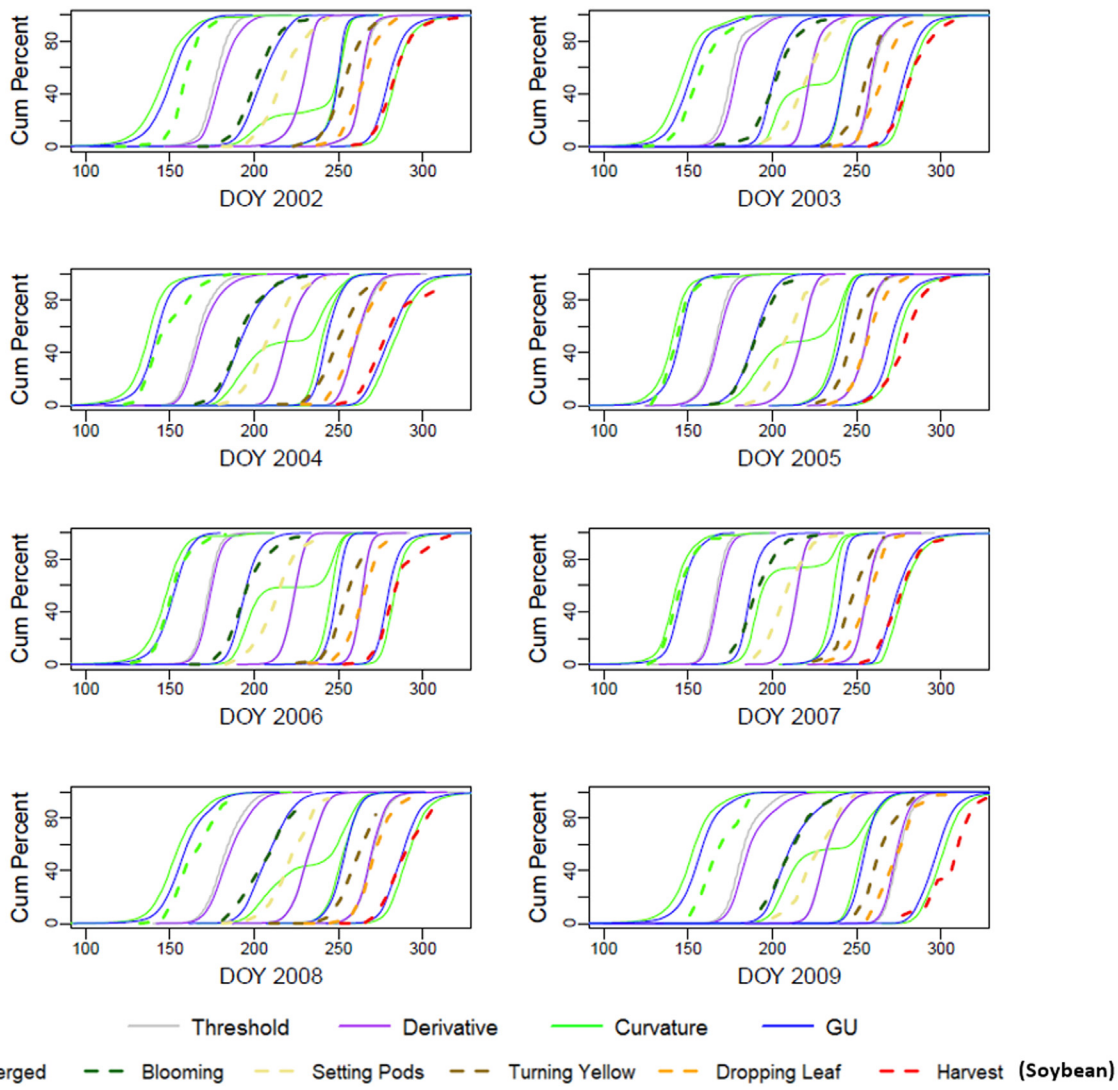

Fig. 9. The cumulative distributions of satellite-Beck-retrieved versus CPR-based crop phenological stages of soybean from 2002 to 2009 throughout Illinois.

ground-observed physiological growing stages of crops. Among the time series phenological models, Beck generally maintained good performance in estimating the phenological transition dates, possibly due to unimodal and clear phenological patterns of crops, though other models might achieve comparable performance in specific stages.

Despite the importance of crop phenology in agronomic monitoring, previous studies have mainly focused on the remote detection of the start and end of growing season. The limited selections of phenological characteristics in those studies may not adequately correspond to the diverse range of crop physiological growing stages, particularly for the dough and dent stages of corn, and setting pods and turning yellow stages of soybean. The difficulty in linking the remotely sensed with ground-based phenological measures remains a major hurdle towards effective crop phenological monitoring. With a combination of 56 phenological characteristics, the framework developed in this study conducts a comprehensive comparison among a wide range of methodologies to optimize the remotely sensed phenological retrieval. It provides a concrete guidance on how various crop phenological stages can be estimated through remotely sensed time series measures. This framework is developed with corn and soybean in Illinois as examples, and can further be evaluated in other regions or for other crops in future studies. It represents a desired first step towards formulating standard crop phenological monitoring protocols via remote sensing.

Under the devised framework, a suite of time series phenological models and time series phenological characterization methods have been evaluated. As both corn and soybean maintain unimodal growing seasons with strong phenological patterns, the four phenological models exhibited comparable performances in a majority of growing stages. In contrast, different phenological characterization methods showed varying accuracies in retrieving similar crop growing stages, or were characteristic of dramatically different stages. Among the phenological characterization methods, the transition dates estimated by threshold-based and derivative-based methods were characteristic of similar crop growing stages, while the transition dates retrieved by curvature-based and Gu-based methods were mostly comparable. More attentions need to be paid to phenological characterization methods for retrieving desired growing stages. Despite the overall good performance of the framework, the silking and dough stages of corn, and the setting pods stage of soybean, exhibited larger differences between remotely sensed and ground-observed dates (i.e., RMSE about 11 days) compared to other physiological stages. For those physiological stages, the integration of the shape model under the framework may further increase the retrieval accuracy, though the calibration of the shape model requires ancillary ground-based crop phenological growth data. Besides, the framework holds strong potentials to be extended to intensified agricultural (e.g., double crops) regions if the crop growth cycle can be delineated. The delineation may benefit from the devised seasonality filtering adjusted for the magnitude threshold of seasonal signals. To be

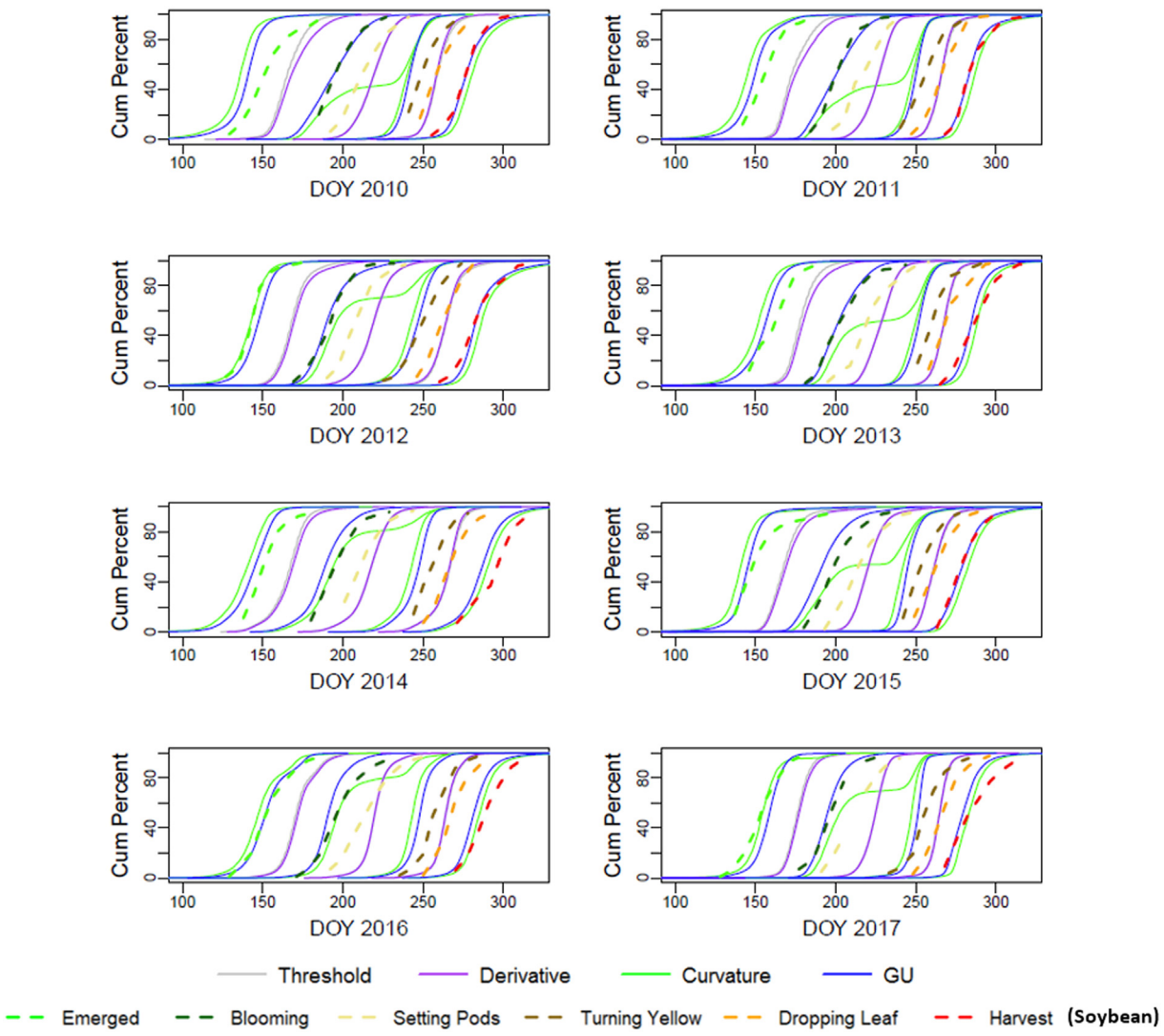

Fig. 10. The cumulative distributions of satellite-Beck-retrieved versus CPR-based crop phenological stages of soybean from 2010 to 2017 throughout Illinois.

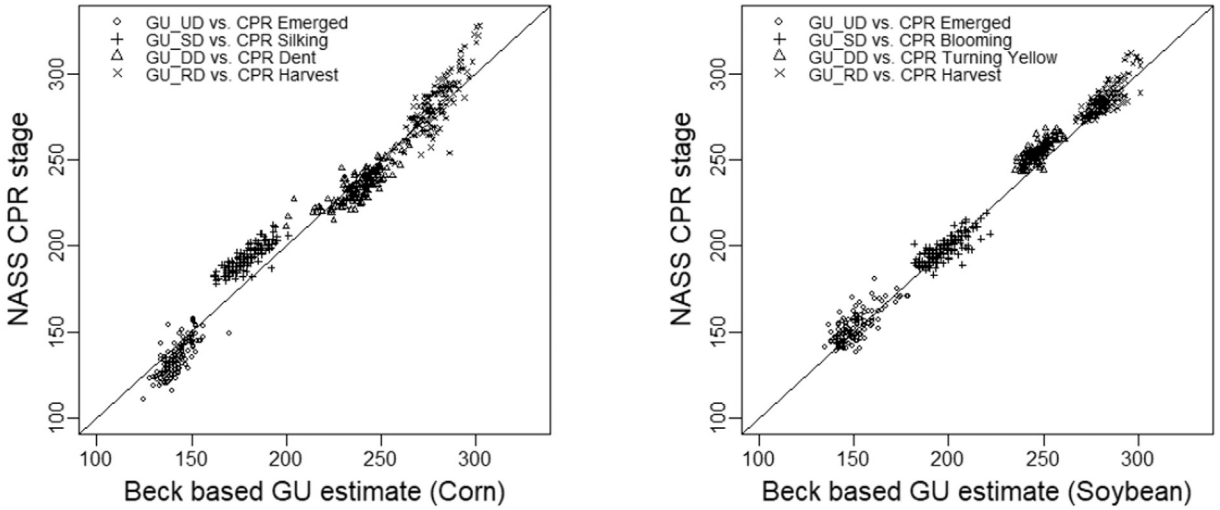

Fig. 11. Comparisons between the median of Beck-Gu retrieved transition dates and the median dates of crops going into corresponding physiological growing stages throughout Illinois at the ASD level from 2002 to 2017.

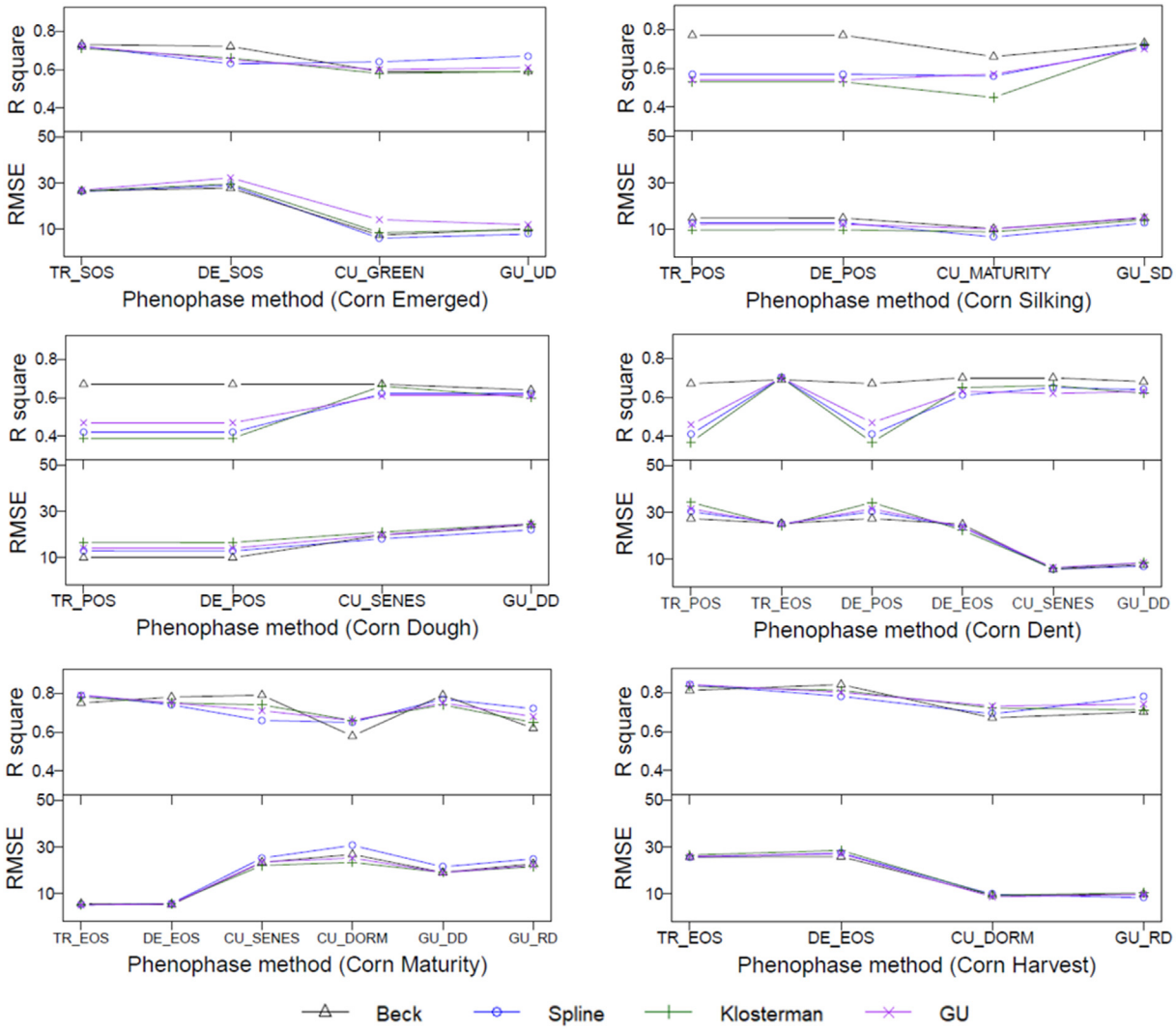

Fig. 12. The RMSE and R squares of the 56 retrieved transition dates of corn at the ASD level in Illinois.

extended to more intensified or diversified agricultural regions, the framework may also benefit from the pheno-network model (Diao, 2019b). The pheno-network model is a non-parametric, complex network-based model that represents the complicated phenological process with a network structure. It may be a desired alternative, particularly in cloud heavily affected or complicated agricultural regions, as the pheno-network model can be constructed with partial-year remote sensing time series.

Validating the remotely retrieved crop phenophases with field phenological measures is challenging, as crop fields are usually proprietary and field phenological observations of crops may not correspond to the spatial resolution of MODIS. As a tradeoff between the state-level and the site-specific ground phenological observations, the ASD-level phenological reference data provide an adequate summary of crop phenological progress over wide geographical regions, as well as accommodate the large-scale spatio-temporal phenological variations within the state. This systematic and consistent dataset collected by NASS is among the most appropriate ones to develop the phenological monitoring framework that can reconcile the remotely sensed with ground-based phenological measures. The MODIS pixels with fractions of corn (or soybean) higher than 90% are selected in this study to balance the pixel purity and sample size for ASD-level crop phenological comparisons. Despite the relatively pure pixels selected, some pixels may have lower corn (or soybean) fractional covers due to the varying pixel footprint sizes at different view angles of MODIS. To further reduce varying pixel footprint influence, aggregating the MODIS data to coarser resolutions (e.g., 1km) might be a solution (Tan et al., 2006). Yet it might dramatically reduce the sample size of relatively pure corn (or soybean) pixels, and the limited samples might not be representative for ASD-level crop phenological comparisons. It would be desired to test the influence of pixel purity, with varying MODIS pixel footprint sizes accommodated, on the phenological detection accuracies in future studies using more adequate ground reference data.

The phenological monitoring framework is developed using the time series of BRDF-corrected MODIS MCD43A4 data. With its high temporal resolution, this daily 16-day composite data from both Terra and Aqua represents an adequate source to monitor the crop phenological progress at regional to global scales, particularly for relatively large crop fields. As for small-holder agricultural systems, the framework can potentially be extended to retrieve the critical phenological transition dates, but with the satellite data of finer spatial and temporal resolutions (e.g., harmonized Landsat and Sentinel-2 [HLS]). The recent advances in retrieving vegetation phenology at 30m spatial resolution using the HLS data can help ease the mixed phenology issue of crops at the field level (Bolton et al., 2020; Gao et al., 2020; Zhang et al., 2020). Also a multitude of data fusion algorithms have been developed to integrate MODIS with finer spatial resolution imagery (e.g., Landsat and Sentinel-2) to generate daily Landsat-wise imagery (Zhu et al., 2018). With the harmonized or fused imagery, the framework can potentially benefit the field-level crop phenological monitoring for small-holder

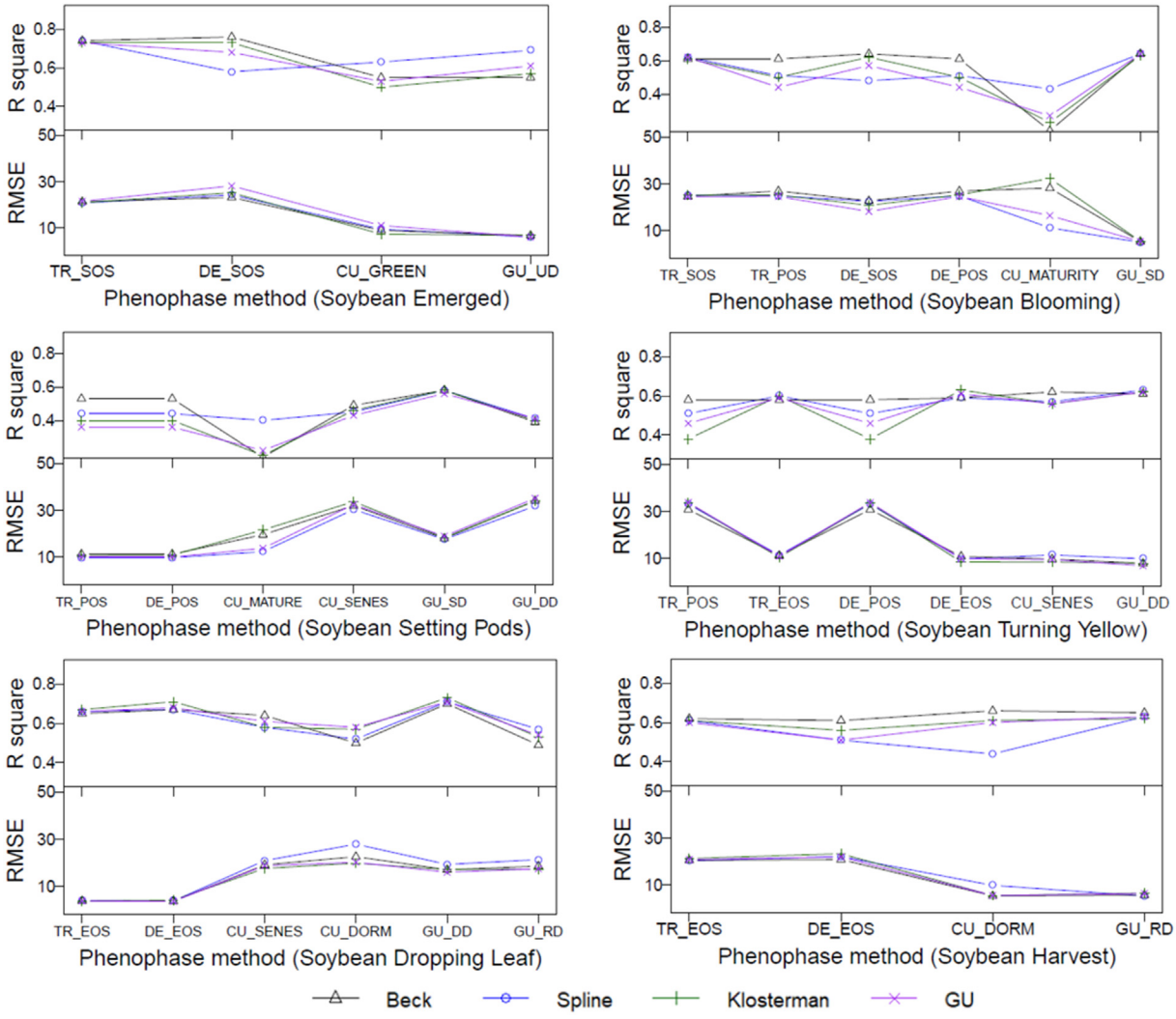

Fig. 13. The RMSE and R squares of the 56 retrieved transition dates of soybean at the ASD level in Illinois.

Table 4
The desired combination of phenological modeling and characterization methods for estimating corn growing stages under the devised framework.

Field stage	Phenological model	Phenological characteristic	R square	RMSE
Emerged	Spline	Gu-based upturn	0.68	7.85
Silking	Beck	Curvature-based maturity	0.66	10.31
Dough	Beck	Derivative-based POS	0.67	9.88
Dent	Beck	Curvature-based senescence	0.7	5.62
Mature	Beck	Derivative-based EOS	0.78	7.5
Harvest	Spline	Gu-based recession	0.78	8.25

Table 5
The desired combination of phenological modeling and characterization methods for estimating soybean growing stages under the devised framework.

Field stage	Phenological model	Phenological characteristic	R square	RMSE
Emerged	Spline	Gu-based upturn	0.68	6.06
Blooming	Spline	Gu-based stabilization	0.64	4.96
Setting pods	Beck	Derivative-based POS	0.53	10.95
Turning yellow	Gu	Gu-based downturn	0.62	6.83
Dropping leaves	Beck	Derivative-based EOS	0.67	5.5
Harvest	Beck	Curvature-based dormancy	0.66	5.33

agricultural systems. Additionally, the development of near-surface remote sensing techniques (e.g., PhenoCam) facilitates the acquisition of consistent and systematic ground phenological observations at field levels, which are complementary to the ASD-level data and can be employed to further evaluate the framework in those agricultural systems.

Among a range of vegetation indices, NDVI has been widely utilized to characterize crop vigor and photosynthetic activities. Under the developed framework, tracking the change of NDVI values throughout the year shows great promise for crop phenological retrieval. Besides NDVI, other vegetation indices (e.g., green chlorophyll vegetation index [GCVI] and wide dynamic range vegetation index [WDRVI]) have also been used in crop studies. Further inspection of those vegetation indices on the retrieval results will facilitate the building of a more robust and comprehensive framework. Overall, the phenological monitoring framework provides a systematic set of methodologies to simultaneously retrieve a wide range of crop physiological growing stages that have marked ecological implications. The wealth of phenological information opens up unique opportunities to investigate how various farm management activities arranged at different crop growing stages affect the crop growth and subsequent productivity. It will also shed light on the shared and divergent effects of climate change or extreme weather conditions on the crop growth at various physiological stages (Wu et al., 2013; Zhou et al., 2017). Those growing stage-specific assessments will potentially enhance our understanding of the complex mechanisms

underlying the crop growth in response to varying environmental stresses, which will help make more adaptive farm management strategies towards sustained agricultural development.

6. Conclusions

The world population will reach about 9.7 billion in the next 30 years, with a rough increase of 83 million people every year. The rapidly growing population will drastically increase the global demand of agricultural crops, posing significant threats to food security. Remote monitoring of crop phenological dynamics in a consistent and systematic manner plays a vital role in optimizing the farm management activities and evaluating the agricultural resilience to extreme weather conditions and future climate change. In this study, we developed a remote sensing phenological monitoring framework that can reconcile satellite-based with ground-based phenological measures. This framework mainly comprises three components: time series phenological preprocessing, time series phenological modeling, and time series phenological characterization. As an exploratory prototype, the framework retrieved a total of 56 phenological transition dates that were subsequently evaluated with ASD-level ground phenological measures. The results indicated that the framework is able to retrieve a wide range of crop physiological growing stages for both corn and soybean, with R square greater than 0.6 and RMSE less than 1 week for most stages. It largely extends the limited satellite phenological measures to a range of phenological transition dates that are characteristic of essential crop growing stages. The phenological monitoring framework shows great promise to enhance our understanding of crop phenological responses to varying environmental stresses, and to help make stage-specific adaptive management strategies to improve crop productivity.

Declaration of Competing Interest

The authors declare that they have no known competing financial interests or personal relationships that could have appeared to influence the work reported in this paper.

Acknowledgements

This work is partially supported by the National Science Foundation under grant 1849821. We would like to thank the University of Illinois at Urbana-Champaign and National Center for Supercomputing Applications for providing the Blue Waters petascale computational resources to conduct this project. We would also like to thank three anonymous reviewers for their constructive comments and suggestions.

Appendix A. Supplementary data

Supplementary data to this article can be found online at https://doi.org/10.1016/j.rse.2020.111960.

References

Asner, G., Townsend, A., Braswell, B.H., 2000. Satellite observation of El Niño effects on Amazon Forest phenology and productivity. Geophys. Res. Lett. 27, 981–984.
Beck, P.S.A., Atzberger, C., Høgda, K.A., Johansen, B., Skidmore, A.K., 2006. Improved monitoring of vegetation dynamics at very high latitudes: A new method using MODIS NDVI. Remote Sens. Environ. 100, 321–334.
Bolton, D.K., Friedl, M.A., 2013. Forecasting crop yield using remotely sensed vegetation indices and crop phenology metrics. Agric. For. Meteorol. 173, 74–84.
Bolton, D.K., Gray, J.M., Melaas, E.K., Moon, M., Eklundh, L., Friedl, M.A., 2020. Continental-scale land surface phenology from harmonized Landsat 8 and Sentinel-2 imagery. Remote Sens. Environ. 240, 111685.
Boryan, C., Yang, Z., Mueller, R., Craig, M., 2011. Monitoring US agriculture: the US Department of Agriculture, National Agricultural Statistics Service, Cropland Data Layer Program. Geocarto Int. 26, 341–358.
Boschetti, M., Stroppiana, D., Brivio, P.A., Bocchi, S., 2009. Multi-year monitoring of rice crop phenology through time series analysis of MODIS images. Int. J. Remote Sens. 30, 4643–4662.
Bradley, B.A., Jacob, R.W., Hermance, J.F., Mustard, J.F., 2007. A curve fitting procedure to derive inter-annual phenologies from time series of noisy satellite NDVI data. Remote Sens. Environ. 106, 137–145.
Brown, M.E., de Beurs, K.M., Marshall, M., 2012. Global phenological response to climate change in crop areas using satellite remote sensing of vegetation, humidity and temperature over 26 years. Remote Sens. Environ. 126, 174–183.
Cleland, E.E., Chuine, I., Menzel, A., Mooney, H.A., Schwartz, M.D., 2007. Shifting plant phenology in response to global change. Trends Ecol. Evol. 22, 357–365.
Diao, C., 2019a. Complex network-based time series remote sensing model in monitoring the fall foliage transition date for peak coloration. Remote Sens. Environ. 229, 179–192.
Diao, C., 2019b. Innovative pheno-network model in estimating crop phenological stages with satellite time series. ISPRS J. Photogramm. Remote Sens. 153, 96–109.
Diao, C., Wang, L., 2016. Incorporating plant phenological trajectory in exotic saltcedar detection with monthly time series of Landsat imagery. Remote Sens. Environ. 182, 60–71.
Dierckx, P., 1995. Curve and Surface Fitting With Splines. Oxford University Press.
Filippa, G., Cremonese, E., Migliavacca, M., Galvagno, M., Forkel, M., Wingate, L., Tomelleri, E., Morra di Cella, U., Richardson, A.D., 2016. Phenopix: A R package for image-based vegetation phenology. Agric. For. Meteorol. 220, 141–150.
Ganguly, S., Friedl, M.A., Tan, B., Zhang, X., Verma, M., 2010. Land surface phenology from MODIS: characterization of the Collection 5 global land cover dynamics product. Remote Sens. Environ. 114, 1805–1816.
Gao, F., Anderson, M.C., Zhang, X., Yang, Z., Alfieri, J.G., Kustas, W.P., Mueller, R., Johnson, D.M., Prueger, J.H., 2017. Toward mapping crop progress at field scales through fusion of Landsat and MODIS imagery. Remote Sens. Environ. 188, 9–25.
Gao, F., Anderson, M., Daughtry, C., Karnieli, A., Hively, D., Kustas, W., 2020. A within-season approach for detecting early growth stages in corn and soybean using high temporal and spatial resolution imagery. Remote Sens. Environ. 242, 111752.
Gu, L., Post, W.M., Baldocchi, D.D., Black, T.A., Suyker, A.E., Verma, S.B., Vesala, T., Wofsy, S.C., 2009. Characterizing the seasonal dynamics of plant community photosynthesis across a range of vegetation types. In: Noormets, A. (Ed.), Phenology of Ecosystem Processes: Applications in Global Change Research. Springer New York, New York, NY, pp. 35–58.
Hermance, J.F., Jacob, R.W., Bradley, B.A., Mustard, J.F., 2007. Extracting phenological signals from multiyear AVHRR NDVI time series: framework for applying high-order annual splines with roughness damping. IEEE Trans. Geosci. Remote Sens. 45, 3264–3276.
Hickman, J., Shroyer, J., 1994. Corn Production Handbook. Publication C, Manhattan.
Jeong, S.-J., Ho, C.-H., Gim, H.-J., Brown, M.E., 2011. Phenology shifts at start vs. end of growing season in temperate vegetation over the Northern Hemisphere for the period 1982–2008. Glob. Chang. Biol. 17, 2385–2399.
Jin, Z., Azzari, G., Lobell, D.B., 2017. Improving the accuracy of satellite-based high-resolution yield estimation: A test of multiple scalable approaches. Agric. For. Meteorol. 247, 207–220.
Johnson, D.M., Mueller, R., 2010. The 2009 Cropland Data Layer. Photogramm. Eng. Remote. Sens. 76, 1201–1205.
Jönsson, P., Eklundh, L., 2004. TIMESAT—a program for analyzing time-series of satellite sensor data. Comput. Geosci. 30, 833–845.
Julitta, T., Cremonese, E., Migliavacca, M., Colombo, R., Galvagno, M., Siniscalco, C., Rossini, M., Fava, F., Cogliati, S., Morra di Cella, U., Menzel, A., 2014. Using digital camera images to analyse snowmelt and phenology of a subalpine grassland. Agric. For. Meteorol. 198-199, 116–125.
Kilgore, G.L., Fjell, D., 1997. Soybean Production Handbook. Publication C-449, Kansas State University Agricultural Experiment Station and Cooperative Extension Service, Manhattan, Kansas, pp. 8–9.
Klosterman, S.T., Hufkens, K., Gray, J.M., Melaas, E., Sonnentag, O., Lavine, I., Mitchell, L., Norman, R., Friedl, M.A., Richardson, A.D., 2014. Evaluating remote sensing of deciduous forest phenology at multiple spatial scales using PhenoCam imagery. Biogeosciences 11, 4305–4320.
Kramer, K., Leinonen, I., Loustau, D., 2000. The importance of phenology for the evaluation of impact of climate change on growth of boreal, temperate and Mediterranean forests ecosystems: an overview. Int. J. Biometeorol. 44, 67–75.
Lauer, J., 2012. The effects of drought and poor corn pollination on corn. Field Crops 28, 493–495.
Lokupitiya, E., Denning, S., Paustian, K., Baker, I., Schaefer, K., Verma, S., Meyers, T., Bernacchi, C.J., Suyker, A., Fischer, M.E., 2009. Incorporation of crop phenology in Simple Biosphere Model (SiBcrop) to improve land-atmosphere carbon exchanges from croplands. Biogeosciences 6, 969–986.
Ma, M., Veroustraete, F., 2006. Reconstructing pathfinder AVHRR land NDVI time-series data for the Northwest of China. Adv. Space Res. 37, 835–840.
Migliavacca, M., Galvagno, M., Cremonese, E., Rossini, M., Meroni, M., Sonnentag, O., Cogliati, S., Manca, G., Diotri, F., Busetto, L., Cescatti, A., Colombo, R., Fava, F., Morra di Cella, U., Pari, E., Siniscalco, C., Richardson, A.D., 2011. Using digital repeat photography and eddy covariance data to model grassland phenology and photosynthetic CO2 uptake. Agric. For. Meteorol. 151, 1325–1337.
Morisette, J.T., Richardson, A.D., Knapp, A.K., Fisher, J.I., Graham, E.A., Abatzoglou, J., Wilson, B.E., Breshears, D.D., Henebry, G.M., Hanes, J.M., Liang, L., 2009. Tracking the rhythm of the seasons in the face of global change: phenological research in the 21st century. Front. Ecol. Environ. 7, 253–260.
Moulin, S., Kergoat, L., Viovy, N., Dedieu, G., 1997. Global-Scale Assessment of Vegetation Phenology Using NOAA/AVHRR Satellite Measurements. J. Clim. 10, 1154–1170.
NASS CDL, 2018. https://www.nass.usda.gov/Research_and_Science/Cropland/metadata/meta.php (last accessed December 15, 2018).
NASS CPR, 2018. https://www.nass.usda.gov/Publications/National_Crop_Progress/ (last

accessed March 1, 2020).
Reed, B.C., Brown, J.F., VanderZee, D., Loveland, T.R., Merchant, J.W., Ohlen, D.O., 1994. Measuring phenological variability from satellite imagery. J. Veg. Sci. 5, 703–714.
Sakamoto, T., Wardlow, B.D., Gitelson, A.A., Verma, S.B., Suyker, A.E., Arkebauer, T.J., 2010. A Two-Step Filtering approach for detecting maize and soybean phenology with time-series MODIS data. Remote Sens. Environ. 114, 2146–2159.
Sakamoto, T., Wardlow, B.D., Gitelson, A.A., 2011. Detecting Spatiotemporal Changes of Corn Developmental Stages in the U.S. Corn Belt Using MODIS WDRVI Data. IEEE Trans. Geosci. Remote Sens. 49, 1926–1936.
Sakamoto, T., Gitelson, A.A., Arkebauer, T.J., 2013. MODIS-based corn grain yield estimation model incorporating crop phenology information. Remote Sens. Environ. 131, 215–231.
Schaaf, C., Wang, Z., 2015a. MCD43A2 MODIS/Terra+ Aqua BRDF/Albedo Quality Daily L3 Global - 500m V006. https://doi.org/10.5067/MODIS/MCD43A2.006. (last accessed March 1, 2020). NASA EOSDIS Land Processes DAAC.
Schaaf, C., Wang, Z., 2015b. MCD43A4 MODIS/Terra+ Aqua BRDF/Albedo Nadir BRDF Adjusted RefDaily L3 Global-500m V006. https://doi.org/10.5067/MODIS/MCD43A4.006. (last accessed March 1, 2020). NASA EOSDIS Land Processes DAAC.
Schaaf, C.B., Gao, F., Strahler, A.H., Lucht, W., Li, X., Tsang, T., Strugnell, N.C., Zhang, X., Jin, Y., Muller, J.-P., Lewis, P., Barnsley, M., Hobson, P., Disney, M., Roberts, G., Dunderdale, M., Doll, C., d'Entremont, R.P., Hu, B., Liang, S., Privette, J.L., Roy, D., 2002. First operational BRDF, albedo nadir reflectance products from MODIS. Remote Sens. Environ. 83, 135–148.
Shen, M., Zhang, G., Cong, N., Wang, S., Kong, W., Piao, S., 2014. Increasing altitudinal gradient of spring vegetation phenology during the last decade on the Qinghai–Tibetan Plateau. Agric. For. Meteorol. 189-190, 71–80.
Tan, B., Woodcock, C.E., Hu, J., Zhang, P., Ozdogan, M., Huang, D., Yang, W., Knyazikhin, Y., Myneni, R.B., 2006. The impact of gridding artifacts on the local spatial properties of MODIS data: Implications for validation, compositing, and band-to-band registration across resolutions. Remote Sens. Environ. 105, 98–114.
Thackeray, S.J., Henrys, P.A., Hemming, D., Bell, J.R., Botham, M.S., Burthe, S., Helaouet, P., Johns, D.G., Jones, I.D., Leech, D.I., Mackay, E.B., Massimino, D., Atkinson, S., Bacon, P.J., Brereton, T.M., Carvalho, L., Clutton-Brock, T.H., Duck, C., Edwards, M., Elliott, J.M., Hall, S.J.G., Harrington, R., Pearce-Higgins, J.W., Høye, T.T., Kruuk, L.E.B., Pemberton, J.M., Sparks, T.H., Thompson, P.M., White, I., Winfield, I.J., Wanless, S., 2016. Phenological sensitivity to climate across taxa and trophic levels. Nature 535, 241.
Viovy, N., Arino, O., Belward, A.S., 1992. The Best Index Slope Extraction (BISE): A method for reducing noise in NDVI time-series. Int. J. Remote Sens. 13, 1585–1590.
Wan, Z., Zhang, Y., Zhang, Q., Li, Z.-l, 2002. Validation of the land-surface temperature products retrieved from Terra Moderate Resolution Imaging Spectroradiometer data. Remote Sens. Environ. 83, 163–180.
Wan, Z., Hook, S., Hulley, G., 2015. MOD11A1 MODIS/Terra land surface temperature/emissivity daily L3 global 1 km SIN grid V006 doi:10.5067/MODIS/MOD11A1.006. (last accessed March 1, 2020) NASA EOSDIS Land Processes DAAC.
Wardlow, B.D., Kastens, J.H., Egbert, S.L., 2006. Using USDA crop progress data for the evaluation of greenup onset date calculated from MODIS 250-meter data. Photogramm. Eng. Remote Sens. 72, 1225–1234.
White, M.A., Thornton, P.E., Running, S.W., 1997. A continental phenology model for monitoring vegetation responses to interannual climatic variability. Glob. Biogeochem. Cycles 11, 217–234.
White, M.A., de Beurs, K.M., Didan, K., Inouye, D.W., Richardson, A.D., Jensen, O.P., O'KEEFE, J., Zhang, G., Nemani, R.R., van Leeuwen, W.J., 2009. Intercomparison, interpretation, and assessment of spring phenology in North America estimated from remote sensing for 1982–2006. Glob. Chang. Biol. 15, 2335–2359.
Wu, J., Zhou, L., Liu, M., Zhang, J., Leng, S., Diao, C., 2013. Establishing and assessing the Integrated Surface Drought Index (ISDI) for agricultural drought monitoring in mid-eastern China. Int. J. Appl. Earth Obs. Geoinf. 23, 397–410.
Xie, Y., Wang, X., Wilson, A.M., Silander, J.A., 2018. Predicting autumn phenology: How deciduous tree species respond to weather stressors. Agric. For. Meteorol. 250-251, 127–137.
Yu, H., Luedeling, E., Xu, J., 2010. Winter and spring warming result in delayed spring phenology on the Tibetan Plateau. Proc. Natl. Acad. Sci. 107, 22151.
Zhang, X., Goldberg, M.D., 2011. Monitoring fall foliage coloration dynamics using time-series satellite data. Remote Sens. Environ. 115, 382–391.
Zhang, X., Zhang, Q., 2016. Monitoring interannual variation in global crop yield using long-term AVHRR and MODIS observations. ISPRS J. Photogramm. Remote Sens. 114, 191–205.
Zhang, X., Friedl, M.A., Schaaf, C.B., Strahler, A.H., Hodges, J.C.F., Gao, F., Reed, B.C., Huete, A., 2003. Monitoring vegetation phenology using MODIS. Remote Sens. Environ. 84, 471–475.
Zhang, X., Wang, J., Henebry, G.M., Gao, F., 2020. Development and evaluation of a new algorithm for detecting 30 m land surface phenology from VIIRS and HLS time series. ISPRS J. Photogramm. Remote Sens. 161, 37–51.
Zhou, J., Jia, L., Menenti, M., 2015. Reconstruction of global MODIS NDVI time series: performance of Harmonic ANalysis of Time Series (HANTS). Remote Sens. Environ. 163, 217–228.
Zhou, L., Wu, J., Mo, X., Zhou, H., Diao, C., Wang, Q., Chen, Y., Zhang, F., 2017. Quantitative and detailed spatiotemporal patterns of drought in China during 2001–2013. Sci. Total Environ. 589, 136–145.
Zhu, X., Cai, F., Tian, J., Williams, T.K.-A., 2018. Spatiotemporal fusion of multisource remote sensing data: literature survey, taxonomy, principles, applications, and future directions. Remote Sens. 10, 527.